

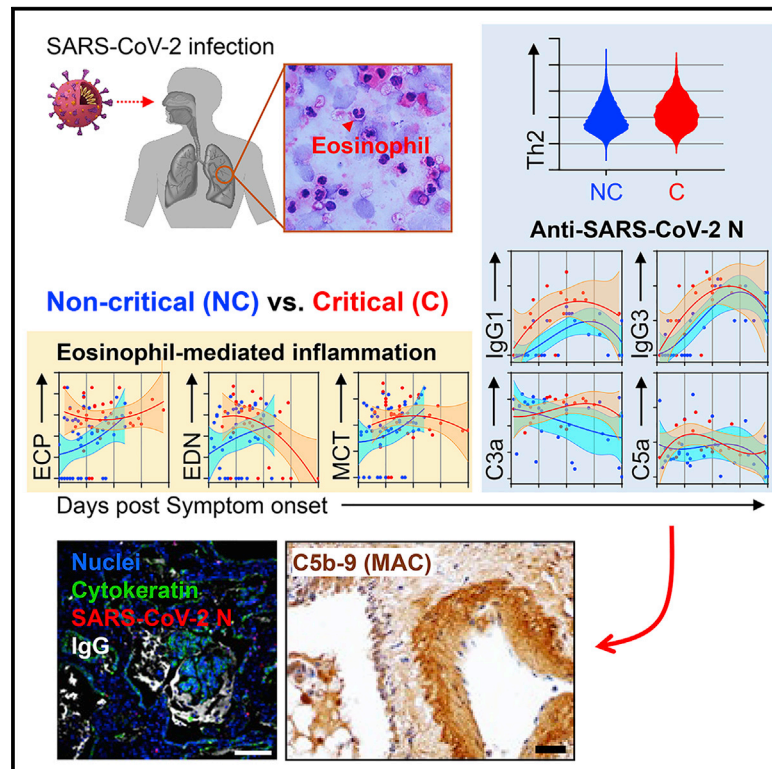


Since January 2020 Elsevier has created a COVID-19 resource centre with free information in English and Mandarin on the novel coronavirus COVID-19. The COVID-19 resource centre is hosted on Elsevier Connect, the company's public news and information website.

Elsevier hereby grants permission to make all its COVID-19-related research that is available on the COVID-19 resource centre - including this research content - immediately available in PubMed Central and other publicly funded repositories, such as the WHO COVID database with rights for unrestricted research re-use and analyses in any form or by any means with acknowledgement of the original source. These permissions are granted for free by Elsevier for as long as the COVID-19 resource centre remains active.

# Enhanced eosinophil-mediated inflammation associated with antibody and complement-dependent pneumonic insults in critical COVID-19

## Graphical abstract



## Authors

Dong-Min Kim, Yuri Kim, Jun-Won Seo, ..., Yoon Kyung Jeon, Yeon-Sook Kim, Nam-Hyuk Cho

## Correspondence

alice@cnuh.co.kr (Y.-S.K.),  
chonh@snu.ac.kr (N.-H.C.)

## In brief

Kim et al. find that critical COVID-19 is associated with enhanced eosinophil-mediated inflammation when compared to non-critical cases. Increased Th2-biased immune responses, accompanying overt complement activation, are seen in the critical group. These findings suggest that enhanced eosinophil-mediated inflammation and dysregulated humoral responses might be drivers of severe COVID-19.

## Highlights

- Critical COVID-19 is associated with enhanced eosinophil-mediated inflammation
- $Fc\gamma R$  signal and complement activation are elevated in critical COVID-19
- Immune complexes and MAC are consistently detected in lung tissues from fatal cases
- Th2-biased humoral responses are associated with critical COVID-19



## Article

# Enhanced eosinophil-mediated inflammation associated with antibody and complement-dependent pneumonic insults in critical COVID-19

Dong-Min Kim,<sup>1,15</sup> Yuri Kim,<sup>2,3,4,15</sup> Jun-Won Seo,<sup>1,15</sup> Jooyeon Lee,<sup>5,15</sup> Uni Park,<sup>2,3,15</sup> Na-Young Ha,<sup>2,3,4,15</sup> Jaemoon Koh,<sup>6,15</sup> Hyoree Park,<sup>2,3</sup> Jae-Won Lee,<sup>2,3</sup> Hyo-Jin Ro,<sup>2,3</sup> Na Ra Yun,<sup>1</sup> Da Young Kim,<sup>1</sup> Sung Ho Yoon,<sup>1</sup> Yong Sub Na,<sup>1</sup> Do Sik Moon,<sup>1</sup> Sung-Chul Lim,<sup>7</sup> Choon-Mee Kim,<sup>8</sup> Kyeongseok Jeon,<sup>2,3</sup> Jun-Gu Kang,<sup>9</sup> Na-Yoon Jang,<sup>2,3</sup> Hyeongseok Jeong,<sup>5</sup> Jungok Kim,<sup>10</sup> Shinhyea Cheon,<sup>5</sup> Kyung Mok Sohn,<sup>5</sup> Jae Youg Moon,<sup>10</sup> Sungmin Kym,<sup>10</sup> Seung Ro Han,<sup>11</sup> Myung-Shin Lee,<sup>11</sup> Hyun-Je Kim,<sup>12</sup> Woong-Yang Park,<sup>12,13</sup> Ji-Yeob Choi,<sup>3</sup> Hyun-Woo Shin,<sup>3</sup> Hye-Young Kim,<sup>3</sup> Chung-Hyun Cho,<sup>3</sup> Yoon Kyung Jeon,<sup>6</sup> Yeon-Sook Kim,<sup>5,\*</sup> and Nam-Hyuk Cho<sup>2,3,4,14,16,\*</sup>

<sup>1</sup>Department of Internal Medicine, Chosun University College of Medicine, Gwangju 61452, Republic of Korea

<sup>2</sup>Department of Microbiology and Immunology, Seoul National University College of Medicine, Seoul 03080, Republic of Korea

<sup>3</sup>Department of Biomedical Sciences, Seoul National University College of Medicine, Seoul 03080, Republic of Korea

<sup>4</sup>Institute of Endemic Disease, Seoul National University Medical Research Center, Seoul 03080, Republic of Korea

<sup>5</sup>Department of Internal Medicine, Chungnam National University School of Medicine, Daejeon 35015, Republic of Korea

<sup>6</sup>Department of Pathology, Seoul National University College of Medicine, Seoul 03080, Republic of Korea

<sup>7</sup>Department of Pathology, Chosun University College of Medicine, Gwangju 61452, Republic of Korea

<sup>8</sup>Premedical Science, Chosun University College of Medicine, Gwangju 61452, Republic of Korea

<sup>9</sup>Korea Zoonosis Research Institute, Jeonbuk National University, Iksan 54531, Republic of Korea

<sup>10</sup>Department of Internal Medicine, Chungnam National University Sejong Hospital, Sejong 30099, Republic of Korea

<sup>11</sup>Department of Microbiology and Immunology, Eulji University School of Medicine, Daejeon 34824, Republic of Korea

<sup>12</sup>Department of Health Sciences and Technology, Samsung Advanced Institute for Health Sciences & Technology, Sungkyunkwan University, Seoul 06351, Republic of Korea

<sup>13</sup>Geninus Inc., Seoul 05836, Republic of Korea

<sup>14</sup>Seoul National University Bundang Hospital, Seongnam-si, Gyeonggi-do 13620, Republic of Korea

<sup>15</sup>These authors contributed equally

<sup>16</sup>Lead contact

\*Correspondence: [alice@cnuh.co.kr](mailto:alice@cnuh.co.kr) (Y.-S.K.), [chonh@snu.ac.kr](mailto:chonh@snu.ac.kr) (N.-H.C.)

<https://doi.org/10.1016/j.celrep.2021.109798>

## SUMMARY

Despite the worldwide effect of the coronavirus disease 2019 (COVID-19) pandemic, the underlying mechanisms of fatal viral pneumonia remain elusive. Here, we show that critical COVID-19 is associated with enhanced eosinophil-mediated inflammation when compared to non-critical cases. In addition, we confirm increased T helper (Th)2-biased adaptive immune responses, accompanying overt complement activation, in the critical group. Moreover, enhanced antibody responses and complement activation are associated with disease pathogenesis as evidenced by formation of immune complexes and membrane attack complexes in airways and vasculature of lung biopsies from six fatal cases, as well as by enhanced hallmark gene set signatures of Fc $\gamma$  receptor (Fc $\gamma$ R) signaling and complement activation in myeloid cells of respiratory specimens from critical COVID-19 patients. These results suggest that SARS-CoV-2 infection may drive specific innate immune responses, including eosinophil-mediated inflammation, and subsequent pulmonary pathogenesis via enhanced Th2-biased immune responses, which might be crucial drivers of critical disease in COVID-19 patients.

## INTRODUCTION

Severe acute respiratory syndrome coronavirus 2 (SARS-CoV-2) has been rapidly spreading worldwide since December 2019 with an average mortality rate of approximately 2.2% (<https://covid19.who.int>). The primary cause of disease fatality is viral pneumonia, resulting in acute respiratory distress syndrome (ARDS) (Yang et al., 2020). Around 80% of confirmed cases are asymptomatic or have mild symptoms, including fever,

cough, sore throat, and myalgia, whereas the rest often develop severe pneumonia requiring supplemental oxygen therapy (Zhou et al., 2020). The most common finding of radiological imaging is bilateral, ground-glass opacity in the periphery of the lungs (Zhou et al., 2020). The mechanisms underlying this varying degree of pneumonia severity observed in COVID-19 patients remain elusive. In particular, the dynamics of pathologic inflammation and the central culprits of pneumonic progression leading to severe ARDS and death still remain unclear, despite numerous



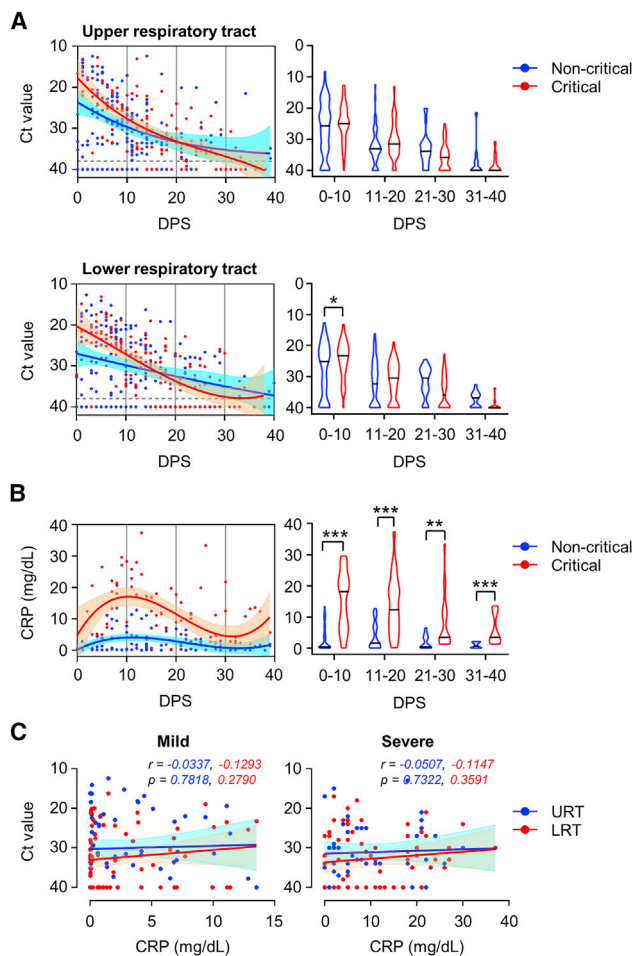


**Figure 1. Kinetic changes of respiratory viral loads and C-reactive proteins (CRPs) in plasma**

(A) Kinetic changes of SARS-CoV-2 viral loads (Ct values) in respiratory specimens. Blue dots ( $n = 196$  for upper and 201 for lower respiratory specimens) from 38 non-critical patients and red dots ( $n = 125$  for upper and 124 for lower respiratory specimens) from 18 critical cases. Blue and red lines indicate non-linear regression with 95% confidence intervals (shaded accordingly). Dashed line indicates cutoff value. Violin plots (right graphs, black line: median) show distribution of total Ct values.

(B) Kinetic change of CRP in plasma. Blue dots from 23 non-critical patients ( $n = 93$ ) and red dots from 10 critical cases ( $n = 84$ ). Violin plots show distribution of CRP levels.

(C) Correlation between viral loads in respiratory specimens and CRP concentration in plasma collected at the same day. Solid lines indicate linear regression with 95% confidence intervals. Pearson's correlation coefficients and linear regression significance are colored accordingly.

$n = 70$  and 68 for non-critical and critical cases, respectively. DPS, days post symptom onset. \* $p < 0.05$ , \*\* $p < 0.01$ , \*\*\* $p < 0.001$ .

studies profiling systemic immune signatures (Lucas et al., 2020).

In order to characterize the pathogenic hallmarks of severe pneumonia in COVID-19 patients, we performed kinetic analysis of inflammatory features of specimens collected from confirmed patients with various degrees of clinical symptoms. We systematically analyzed inflammatory components and leukocytes in

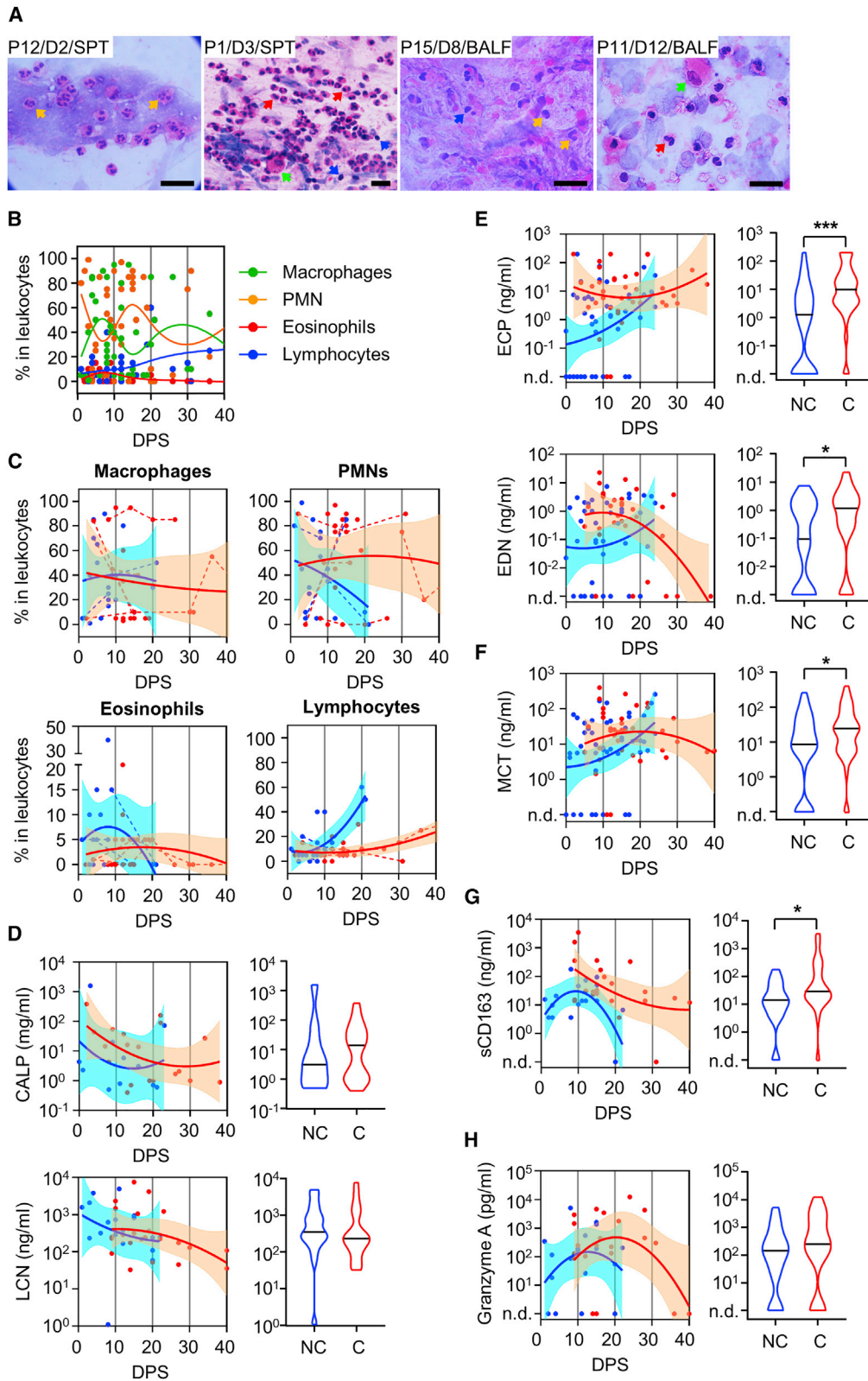
bronchoalveolar lavage fluids (BALFs), sputa, lung tissue biopsies, and blood to characterize kinetic responses of pulmonary inflammation upon viral infection. We also assessed the hallmark gene set scores for related signaling pathways using gene expression datasets from recent single-cell RNA sequencing (scRNA-seq) studies in respiratory leukocytes from COVID-19 patients (Chua et al., 2020; Liao et al., 2020). This extensive analysis revealed that critical COVID-19 is associated with enhanced eosinophil-mediated pulmonary inflammation, as identified by cytological analysis and detection of granular contents derived from the inflammatory cells. In addition, kinetic profiling of inflammatory mediators, including various cytokines and chemokines, and titration of antibodies against a viral antigen revealed emerging T helper (Th2)-biased adaptive immune responses, coupled to overt complement activation, especially in the critical group. Moreover, we observed extensive immune complexes and membrane attack complexes in pulmonary airways and vasculatures of lung biopsies from six fatal cases. These results suggest that SARS-CoV-2 infection may drive scripted specific innate immune responses, including eosinophil-mediated inflammation, and subsequent Th2-biased antigen-specific immune responses, which may contribute to COVID-19-associated severe pneumonia.

## RESULTS

### Viral loads and disease severity of COVID-19

Baseline characteristics of the confirmed patients included in this study are summarized in Table S1. The non-critical group includes 50 patients who were asymptomatic, with mild respiratory symptoms but no detectable pneumonia, or with mild to severe pneumonia as determined by chest imaging and clinical symptoms. The critical group includes 25 patients who suffered from ARDS or other critical conditions requiring high-flow oxygen supply and/or mechanical ventilation. Among the critical patients, 16 patients survived and were discharged, whereas 9 patients (P15, P68–P75) succumbed to death due to fatal ARDS. The patients were also divided into two sets. Group 1 includes 15 patients (10 non-critical and 5 critical group patients) who provided blood and respiratory specimens at different time points after symptoms onset. Group 2 includes 60 patients (40 non-critical and 20 critical patients) who provided respiratory specimens during the acute phase of COVID-19. Lung biopsies were obtained from six fatal cases (P15, P71–P75) at the indicated time after death.

First, we investigated the potential association of viral loads of respiratory secretions with systemic inflammation, as indicated by the levels of C-reactive proteins (CRPs) in plasma (Li et al., 2020). The kinetics of viral loads in respiratory specimens generally showed higher levels of viral RNA in the critical group than in non-critical cases during the first 10 days after symptom onset, but they were not significantly different thereafter (Figure 1A). In particular, the levels of viral RNA were significantly higher in lower (sputa and BALFs) respiratory tracts of the critical group than those of non-critical cases during the early phase of symptom onset. In addition, the levels of CRPs in plasma were more significantly elevated in critical patients, especially during the first 20 days after symptom onset, with a peak around day 10



(legend on next page)

(D10) (Figure 1B). However, a comparison of viral loads in respiratory specimens and CRP levels in plasma collected on the same days did not reveal any significant correlation (Figure 1C). In addition, when we investigated the potential association of viral loads in respiratory specimens with patients' age (younger group defined as less than 60 years and elderly group as 60 years and over) and disease severity, there was a significantly higher viral load in elderly patients than in the younger group with non-critical disease, whereas there was no significant difference between the age groups with critical COVID-19 nor between severity within the same age group (Figures S1A and S1B). Nevertheless, we noticed rather delayed clearance of viral RNA in elderly patients with critical disease. Therefore, viral loads measured in respiratory secretions during the symptomatic period may not be significantly associated with systemic inflammation and disease severity in COVID-19 patients.

### Cytological analysis of respiratory specimens

To investigate the potential causative factors driving severe pulmonary inflammation during the acute phase of COVID-19, we tried to directly analyze the inflammatory cells and mediators in respiratory specimens. 45 BALFs and sputa samples collected from patient groups 1 and 2 at various time points after symptom onset were analyzed by H&E staining to identify types and proportions of immune cell subsets infiltrating infected lungs (Figures 2A and 2B; Table S2). Despite a wide variation among the specimens, BALFs and sputa from COVID-19 patients mainly contained polymorphonuclear cells (PMNs) (mostly neutrophils, mean  $\pm$  SD: 46.8%  $\pm$  34.3% in total leukocytes), monocytes/macrophages (37.5%  $\pm$  32.7%), and a few lymphocytes (11.6%  $\pm$  12.2%). We also observed eosinophils (4.3%  $\pm$  7.3%) in 48.9% (22/45) of the respiratory specimens (Figures 2A and 2B; Table S2). When we compared the level of each inflammatory cell type between non-critical and critical patients, the relative proportion of all of the cell types were not significantly different between the groups, although eosinophils were slightly higher in the non-critical group (6.0%  $\pm$  9.4%) than in critical patients (2.8%  $\pm$  4.6%,  $p = 0.18$ ) (Table S2).

To assess the kinetic changes of immune cell types in respiratory specimens of COVID-19 patients, the relative proportion of each cell type was measured over time after symptom onset by H&E staining (Figures 2B and 2C). Despite individual variations and fluctuations among the specimens, PMN levels, primarily neutrophils, were sustained in respiratory specimens from critical cases, but they rapidly declined in non-critical

patients during the first 20 days after symptom onset. Monocytes/macrophages also gradually decreased after an initial peak around D10 after symptom onset in both critical and non-critical groups, whereas lymphocytes gradually increased more rapidly in non-critical patients than in the critical group (Figure 2C). Interestingly, eosinophils were detectable in 55% (11/20) of specimens from non-critical patients during the first 10 days after symptom onset, whereas their infiltration was rather delayed and peaked during D10–D20 in critical cases (Figure 2C). The eosinophil-positive rate in critical patient samples was 44.0% (11/25) when assessed by H&E.

### Enhanced eosinophil-mediated inflammation in critical COVID-19 patients

Since we observed pulmonary infiltration of PMNs, including neutrophils and eosinophils, we measured the levels of inflammatory mediators derived from neutrophils (lipocalin-2 [LCN], calprotectin [CALP]) (Pechous, 2017) and eosinophils (eosinophil-derived neurotoxin [EDN], eosinophilic cationic protein [ECP]) (Rosenberg et al., 2013) in the respiratory specimens to assess innate cellular activation. The relative levels of LCN and CALP were not significantly different between non-critical (mean  $\pm$  SD: 806.4  $\pm$  1,232.6 ng/mL and 155.3  $\pm$  478.7 mg/mL for LCN and CALP, respectively) and critical groups (770.0  $\pm$  1,658.0 ng/mL and 44.7  $\pm$  91.1 mg/mL for LCN and CALP, respectively) (Figure 2D), although neutrophil responses were more sustained in critical cases (Figure 2C). In contrast, the levels of ECP and EDN were significantly higher in the respiratory specimens from critical patients (mean  $\pm$  SD: 38.9  $\pm$  62.1 and 2.7  $\pm$  4.8 ng/mL for ECP and EDN, respectively) than in those from non-critical cases (11.0  $\pm$  31.9 and 1.0  $\pm$  1.5 ng/mL for ECP and EDN, respectively) (Figure 2E). In addition, the level of mast cell tryptase (MCT) derived from mast cells upon activation was also significantly higher in the critical group (51.7  $\pm$  82.0 ng/mL) than in non-critical cases (29.6  $\pm$  49.6 ng/mL) (Figure 2F). We also examined macrophage activation syndrome by measuring soluble CD163 (sCD163) molecules in the respiratory samples (Shoenfeld, 2020). The levels of sCD163 peaked at around D10 in both non-critical and critical groups (Figure 2G). The peak response was higher in critical cases than in the non-critical group, and the overall levels were significantly enhanced in critical patients, as previously suggested (Shoenfeld, 2020). This confirms the role of macrophage infiltration and activation, potentially with a M2 phenotype, during the early phase of critical COVID-19 pneumonia

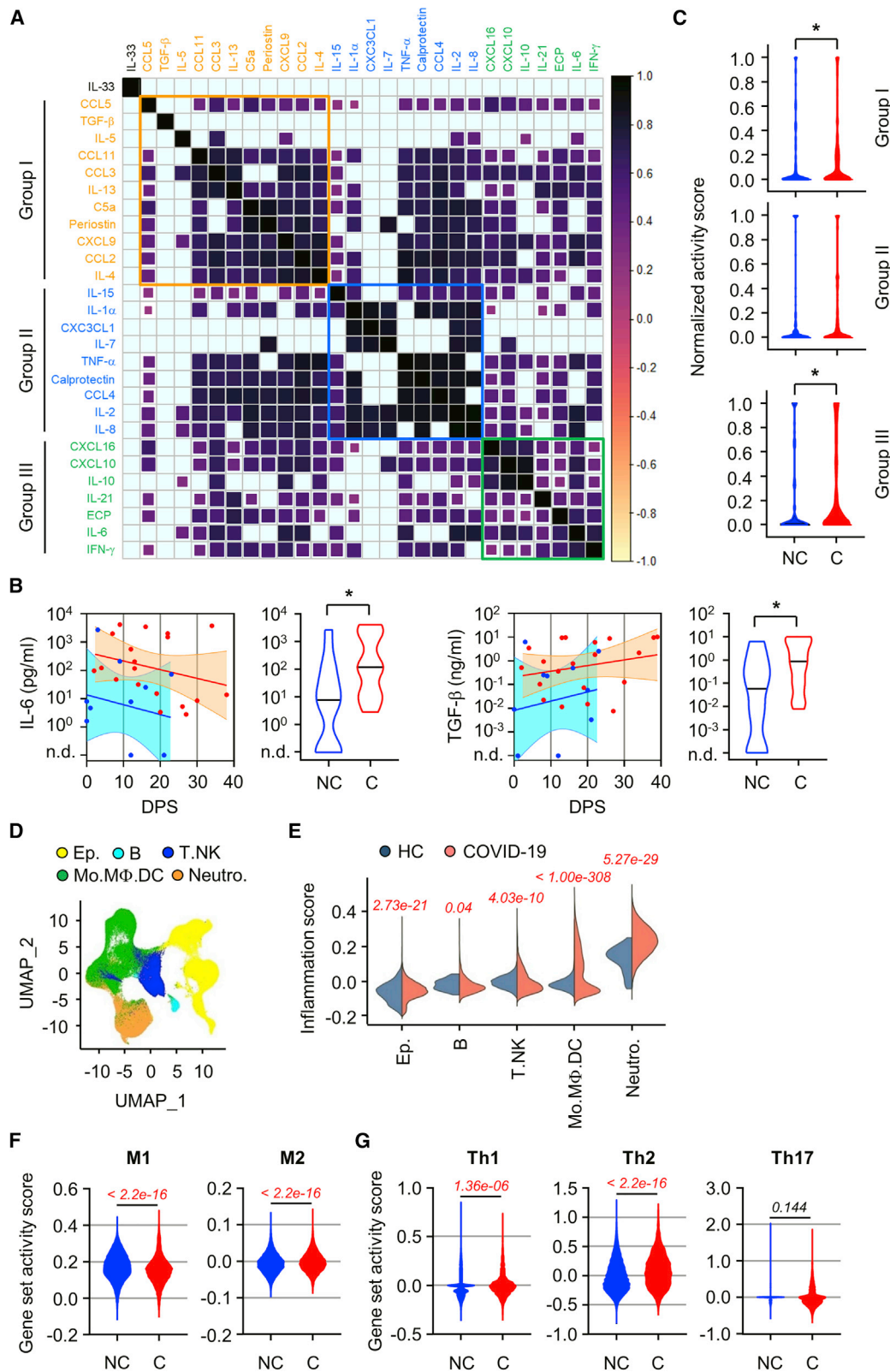
### Figure 2. Kinetic changes of respiratory leukocytes and their activities in respiratory specimens collected from COVID-19 patients

(A) Cytological analysis of sputum (SPT) and bronchoalveolar lavage fluid (BALF) by H&E staining. The patient's ID, collection day after symptom onset, and types of specimens (SPT and BALF) are presented. Orange arrows indicate PMNs (mostly neutrophils); red arrows indicate eosinophils; blue arrows indicate lymphocytes; and green arrow indicate macrophages. Scale bars, 20  $\mu$ m.

(B) Kinetic changes of the indicated leukocytes in respiratory specimens. Colored lines indicate smoothing splines.  $n = 45$ .

(C) Kinetic changes in relative frequencies of the indicated leukocyte subsets in non-critical (blue,  $n = 20$ ) and critical (red,  $n = 25$ ) groups. Solid lines indicate non-linear regression with 95% confidential intervals. Dashed lines indicate data points from individual patients.

(D–H) Kinetic changes of inflammatory markers derived from neutrophils (D), eosinophils (E), mast cells (F), macrophages (G), and cytotoxic T cells/NK cells (H) in respiratory specimens. Solid lines indicate non-linear regression with 95% confidential intervals. Violin plots show distribution of inflammatory marker levels in non-critical (NC) and critical (C) cases. ECP, eosinophilic cationic protein ( $n = 48$  for non-critical and 36 for critical cases); EDN, eosinophil-derived neurotoxin ( $n = 43$  for non-critical and 31 for critical cases); MCT, mast cell tryptase ( $n = 51$  for non-critical and 38 for critical cases); LCN, lipocalin-2 ( $n = 24$  for non-critical and 26 for critical cases); CALP, calprotectin ( $n = 11$  for non-critical and 19 for critical cases); sCD163 and granzyme A ( $n = 18$  for non-critical and 23 for critical cases). \* $p < 0.05$ , \*\*\* $p < 0.001$ .



(legend on next page)

(Zeng et al., 2020). In addition, cytotoxic activity of cytotoxic T lymphocytes (CTLs) and natural killer (NK) cells was not significantly different between critical and non-critical groups, when assessed by measuring granzyme A in respiratory specimens (Figure 2H). These results show that there is an acute spike in macrophage activation during the early phase of critical COVID-19 pneumonia and highlight the significant contribution of enhanced and sustained eosinophil-mediated inflammation (Merad and Martin, 2020).

When we compared the levels of inflammatory mediators between the younger ( $\leq 59$ ) and older age ( $\geq 60$ ) group, the only significant difference was in EDN, which was significantly higher in the younger group than in elderly patients (Figures S1C–S1I). However, the difference was not significant when they were further accounting for disease severity (Figure S1H). Nevertheless, it is interesting to note that the levels of ECP were significantly higher in elderly patients than in younger patients with critical COVID-19 (Figure S1G).

We also assessed the potential correlation of inflammatory mediators with viral loads in the same respiratory specimens. Regardless of disease severity, viral load was significantly correlated with levels of LCN, indicating a functional association of neutrophilic inflammation with viral load (Figure S2A). However, the indicator of eosinophil-mediated inflammation, ECP, was not positively correlated with viral load. In addition, both MCT and sCD163 were not significantly correlated with viral load. These data suggest that enhanced eosinophil-mediated inflammation, as well as mast cell and macrophage activation, might be associated with host factors, rather than the degree of viral replication in lower respiratory tracts.

Additionally, we validated plasma exudation in lower respiratory specimens by measuring the concentration of  $\alpha_2$ -macroglobulin and albumin (Persson, 2019).  $\alpha_2$ -Macroglobulin, an index of plasma leakage, was detected by ELISA in all the respiratory samples ( $n = 40$ , mean  $\pm$  SD:  $140.0 \pm 632.6 \mu\text{g/mL}$ ), and albumin was also detected by a colorimetric assay (detection limit:  $0.1 \text{ g/dL}$ ) in 86.4% of samples ( $n = 44$ , mean  $\pm$  SD:  $0.83 \pm 1.51 \text{ g/dL}$ ) (Figures S2B–S2E). The levels of  $\alpha_2$ -macroglobulin and albumin in respiratory specimens were slightly higher in critical COVID-19 patients than in the non-critical group, but the differences were not statistically significant (Figures S2B and S2D). Their concentrations did not significantly correlate with viral load measured in the same specimen, whereas the levels of both indicators were significantly correlated with the levels of ECP regardless of disease severity (Figures S2C and S2E). In addition, the level of  $\alpha_2$ -macroglobulin

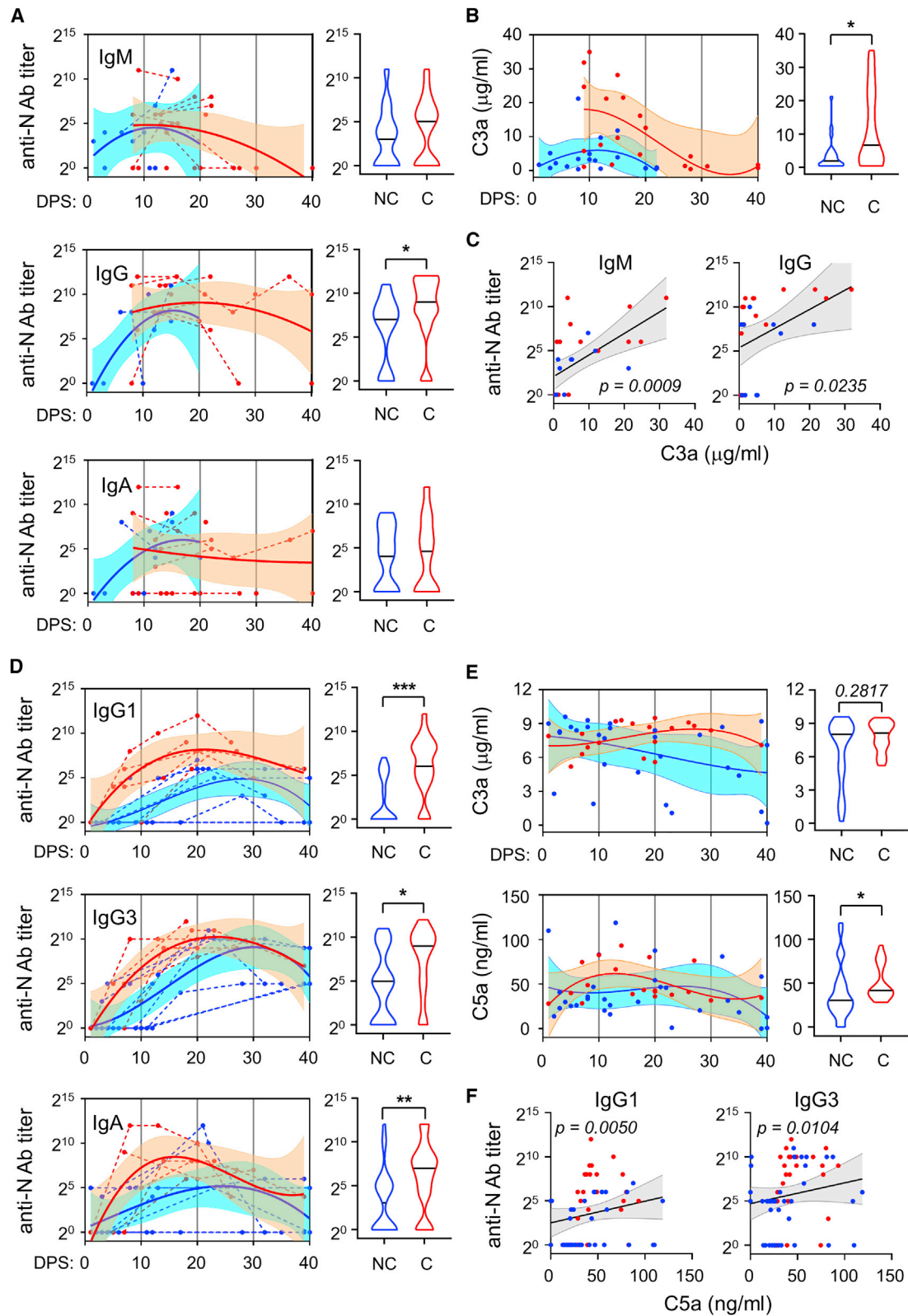
with high molecular weight (720 kDa) was significantly correlated with the concentrations of albumin (69 kDa) measured in the same specimen (Figure S2F), indicating an indiscriminate microvascular-epithelial passage of macromolecules and non-sieved nature of plasma exudation responses in the inflamed lung (Persson, 2019).

### Characterization of pulmonary inflammation in COVID-19 patients

To further define pulmonary inflammation associated with COVID-19 patients, we examined multiple cytokines, chemokines, and inflammatory mediators in 31 respiratory samples, including sputa and BALFs, collected from 11 patients (6 non-critical cases and 5 critical cases in group 1) at various time points after symptom onset (Figure 3A; Figure S3). When we assessed the overall levels of these soluble proteins and grouped them by a hierarchical clustering based on the correlation coefficients of proteins, three distinct families of immune markers positively correlated with each other, although many of them showed broad positive correlation with outgroup members (Figure 3A). Group I includes interleukin (IL)-4, IL-5, IL-13, transforming growth factor (TGF)- $\beta$ , CCL2 (MCP-1), CCL3 (MIP-1 $\alpha$ ), CCL5 (RANTES), CCL11 (Eotaxin-1), CXCL9 (MIG), C5a, and periostin; group II contains IL-1 $\alpha$ , IL-2, IL-7, IL-8, IL-15, tumor necrosis factor (TNF)- $\alpha$ , CCL4 (MIP-1 $\beta$ ), CX3CL1 (Fractalkine), and calprotectin; and group III includes IL-6, IL-10, IL-21, interferon (IFN)- $\gamma$ , CXCL10 (IP-10), CXCL16, and ECP. It is notable that group I includes type 2 cytokines (IL-4, IL-5, IL-13, and TGF- $\beta$ ) and chemoattractants (CCL3, CCL5, CCL11, periostin, and C5a) for granulocytes, including eosinophils (Rosenberg et al., 2013). Alternatively, group II primarily includes various cytokines linked to T cell homeostasis and inflammatory cytokines (IL-2, IL-7, IL-15, IL-1 $\alpha$ , IL-8, and TNF- $\alpha$ ), while group III includes cytokines and chemokines involved in cell-mediated immunity (IL-6, IL-10, IL-21, IFN- $\gamma$ , CXCL10, and CXCL16), indicating a functional correlation of soluble mediators in the inflamed respiratory environment during the acute phase of COVID-19. When we compared the overall levels of cytokines and chemokines between critical and non-critical groups, only three inflammatory markers, IL-6 (mean  $\pm$  SD:  $2.8 \pm 8.1$  versus  $9.1 \pm 14.1 \text{ ng/mL}$  for the non-critical and critical group, respectively), TGF- $\beta$  ( $0.9 \pm 1.9$  versus  $3.2 \pm 4.0 \text{ ng/mL}$  for the non-critical and critical group, respectively), and ECP (as noted above), were significantly higher in critical patients than in the non-critical group (Figure 3B; Figure S3). Systemic elevation of IL-6 is known to be a hallmark of respiratory failure and cytokine release syndrome in severe

### Figure 3. Correlation of respiratory inflammatory mediators and gene set activity scores of respiratory leukocytes in COVID-19 patients

- (A) Correlation matrix of 28 inflammatory proteins detected in respiratory samples. The size of the squares and the intensity of color are proportional to Spearman correlation coefficients. Only significant correlations ( $p < 0.05$ ) are presented. Groups I–III are defined by hierarchical clustering.
- (B) Kinetic changes of IL-6 and TGF- $\beta$ . Non-critical (blue, NC,  $n = 11$ ) and critical (red, C,  $n = 20$ ) groups. Solid lines indicate linear regression with 95% confidential intervals. Violin plots show distribution of the cytokine levels.
- (C) Normalized activity scores of inflammatory proteins for each group. Blue indicates non-critical patients; red indicates critical patients. \* $p < 0.05$ .
- (D) UMAP presentation of major cell types and associated clusters in respiratory leukocytes. Ep., epithelial cells; B, B cells; T.NK, T and NK cells; Mo.MF.DC, monocytes, macrophages, and dendritic cells; Neutro., neutrophils.
- (E) Hallmark gene set scores for inflammatory responses, computed for the indicated leukocyte subsets. HC, healthy control.
- (F) Computed hallmark gene set activity scores of M1 and M2 phenotypes in the mononuclear phagocyte population (monocytes, macrophages, and dendritic cells).
- (G) Hallmark gene set activity scores of Th1, Th2, and Th17 responses in T cells.  $p$  values for differences between indicated groups are presented.



(legend on next page)

COVID-19 (Gubernatorova et al., 2020; Mazzoni et al., 2020). Our data confirm a significant association of this inflammatory cytokine with disease severity even in the respiratory environment of COVID-19 patients. In addition, IL-6 was broadly and significantly associated with pro-inflammatory cytokines, as well as type 2 cytokines. ECP was significantly correlated with pro-inflammatory cytokines, including IL-1 $\alpha$ , IL-6, and TNF- $\alpha$ , in addition to type 2 cytokines, such as IL-4 and IL-13 (Figure 3A), suggesting a potential association of eosinophil-mediated inflammation with cytokine release syndrome and type 2 immune responses. TGF- $\beta$  was barely correlated with any other soluble markers, although it was grouped with type 2 cytokines. Given the functional role of TGF- $\beta$  in mucosal immunity and eosinophil-mediated pneumonia (Borsutzky et al., 2004), a significant elevation of TGF- $\beta$  in respiratory specimens from severe COVID-19 patients may denote eosinophil-mediated and type 2 mucosal immune responses. Indeed, when we compared normalized activities of all soluble markers between critical and non-critical cases, the inflammatory mediators in group I and III were significantly higher in critical patients than in non-critical cases, whereas those in group II were not significantly different (Figure 3C).

To further confirm enhanced type 2 mucosal immune responses, we retrieved gene expression datasets from recent scRNA-seq studies using respiratory leukocytes from COVID-19 patients (Chua et al., 2020; Liao et al., 2020) and analyzed hallmark gene set scores for each signaling pathway (Pont et al., 2019). In the initial analyses of signature gene set scores for inflammation in major leukocyte populations (Figure 3D), myeloid cells, including monocytes, macrophages, and dendritic cells, as well as neutrophil hallmark inflammation scores were prominently increased when compared to those of the healthy control group (Figure 3E). Analysis of scRNA-seq datasets from mononuclear phagocytes (monocytes, macrophages, and dendritic cells) showed significantly higher levels of hallmark gene set scores for M1 phenotype in the non-critical group than those of critical cases, while conversely the gene set scores for M2 phenotype were significantly increased in critical cases than in the non-critical group (Figure 3F). In addition, the hallmark gene set scores for Th2 responses were significantly elevated in the critical group than in non-critical cases (Figure 3G). Those for Th1 responses were also generally higher in critical patients than in the non-critical group, whereas the difference for Th17 responses was not statistically significant between non-critical and critical patients. These results clearly and consistently indicate that Th2 type immune responses, as well as the M2 type-biased phagocytic cell phenotype, are enhanced in the respiratory environment of critical cases compared to the non-critical group.

### Enhanced antibody responses and complement activation in critical COVID-19

Since eosinophilic inflammation is associated with Th2-polarized immune responses in various pulmonary disorders (De Giacomo et al., 2018; Rosenberg et al., 2013), we next assessed viral antigen-specific antibody responses in respiratory secretions and plasma from the patients, with a focus on specific isotypes. Antibody responses against SARS-CoV-2 nucleocapsid (N) protein generally increased during the first 10 days after symptom onset, peaking at D10–D20 before gradually declining in the respiratory specimens, regardless of disease severity (Figure 4A). While immunoglobulin (Ig)G was significantly higher in critical cases, especially during D10–D20, there was no significant difference in all other isotype responses against the viral antigen. Since several reports have shown elevated complement activation in the plasma of critical COVID-19 patients (Carvelli et al., 2020; Cugno et al., 2020; Wu et al., 2020), we also assessed the levels of complement protein in the respiratory specimens. We detected significantly higher levels of C3a with a peak response at around D10 in critical patients (Figure 4B), indicating concomitant complement activation with antibody responses in the respiratory tract during the acute phase of COVID-19. In order to examine antibody-dependent activation of the complement pathway (Wu et al., 2020), we examined the correlation of C3a concentration with anti-N IgM and IgG antibody responses, which are the major isotypes involved in the classical pathway of complement activation (Ricklin et al., 2016). The concentration of C3a was significantly correlated with both IgM and IgG levels in the same respiratory specimen (Figure 4C), suggesting that activation of the classical pathway leads to complement activation in the respiratory tract in critical COVID-19.

Next, we examined the systemic levels of antigen-specific antibody responses in plasma (Figure 4D). Anti-N IgG1 and IgG3 antibodies gradually increased in the plasma of all 15 patients (10 non-critical and 5 critical patients) examined, but IgG2 and IgG4 were barely detected. Specific IgA responses were detected in plasma from all of the critical patients and were positive in 70% of non-critical patients. Antibody responses were generally more prompt and pronounced in critical cases than in the non-critical group (Figure 4D). Moreover, levels of all of the antibody isotypes examined were significantly higher in the critical group than in non-critical patients. We also assessed complement activation in the same set of plasma samples by measuring the concentrations of C3a and C5a. As observed in respiratory specimens, levels of C3a and C5a were generally higher in plasma from critical patients ( $7.9 \pm 1.3 \mu\text{g/mL}$  and  $50.5 \pm 20.3 \text{ ng/mL}$  for C3a and C5a, respectively) than from the non-critical group ( $1.2 \pm 2.0 \mu\text{g/mL}$  and

#### Figure 4. Kinetic changes of SARS-CoV-2 N-specific antibodies and complement activation in respiratory tracts and plasma

(A and B) Kinetic changes in specific antibody responses against viral N protein (A) and C3a (B) in respiratory samples. Blue indicates non-critical (n = 13 for antibodies and 20 for C3a); red indicates critical (n = 28 for antibodies and 20 for C3a); solid lines indicate non-linear regression with 95% confidential intervals. (C) Correlation of C3a levels with N-specific IgM and IgG. Solid lines indicate linear regression with 95% confidential intervals. p values were determined by a Spearman's rank test. n = 27. (D and E) Kinetic changes in specific antibody responses against viral N protein (D), C3a, and C5a (E) in plasma samples. Blue indicates non-critical (n = 30); red indicates critical (n = 18); solid lines indicate non-linear regression with 95% confidential intervals. Dashed lines (A and D) indicate data points from individual patients. Violin plots show levels in NC and C cases. \*p < 0.05, \*\*p < 0.01, \*\*\*p < 0.001. (F) Correlation of C5a levels with N-specific IgG1 and IgG3. Solid lines indicate linear regression. p values were determined by a Spearman's rank test. n = 61.

38.9 ± 30.1 ng/mL for C3a and C5a, respectively) (Figure 4E). The difference in C5a levels between critical and non-critical groups was statistically significant, as previously reported (Carvelli et al., 2020). In addition, we observed a significant positive correlation of C5a levels with plasma IgG1 and IgG3 levels (Figure 4f). These results confirm that viral antigen-specific antibody responses are significantly higher in plasma from critical patients than from the non-critical group, as previously reported (Long et al., 2020; Wang et al., 2020b). This might be functionally linked to systemic and persistent activation of the complement cascade in severe pneumonic patients, potentially through the classical pathway. In addition, a systemic but respiratory surge of viral antigen-specific antibody responses, driven by enhanced eosinophil-mediated inflammation and TGF- $\beta$  responses in the respiratory tract, could be a hallmark of pathogenic progression and Th2-biased mucosal immunity in pneumonic lungs of critical COVID-19 patients.

#### Pathogenic role of antibody responses and complement activation in critical COVID-19

In order to confirm the pathogenic contribution of antibody responses and complement activation in critical COVID-19, we performed immunohistological and immunofluorescence analysis of two lung biopsies obtained during late stage (D36 and D48) of a fatal case, P15, before succumbing to death at D60 (Figures 5A and 6A). Formalin-fixed paraffin-embedded lung tissue subjected to immunohistochemical staining with anti-C5b-9 antibody showed massive deposition of membrane attack complexes (MACs) in vascular walls, particularly subendothelial and smooth muscle layers, bronchial epithelial cells, as well as inflammatory cells, including macrophages and lymphocytes (Figure 5A). The intensity of C5b-9 staining in pulmonary vessels was increased at D48 when compared to that of D38. We also detected fixed C3b fragments in vascular walls, bronchial epithelia, pneumocytes, and interstitia of inflamed lung tissues (Figure S4A). Moreover, deposition of IgG immune complexes in hyaline membranes and fibrin deposits within luminal spaces of airways and vascular capillaries emerged at D36 and increased at D48 (Figure 6A; Figure S4B). These results strongly suggest that concomitant immune complex formation and complement activation may drive irreversible pulmonary damage in fatal COVID-19. We further confirmed immune complex formation and complement activation obtained in lung biopsies from five fatal cases of COVID-19 shortly after death (Figures 5B and 6B), strongly suggesting general pathogenic contribution of antibody responses and complement activation in fatal COVID-19. Viral N antigen was barely detected in these final-stage autopsies. Analysis of lung biopsies from two fatal idiopathic pulmonary fibrosis (IPF) cases supported by extracorporeal membrane oxygenation (ECMO) was also performed as positive controls because abnormalities of humoral immunity, involving immune complexes and complement activation, are common in severe IPF patients (Kahloon et al., 2013). In lung biopsies of the fatal IPF patients without COVID-19, IgG-positive immune complexes were present in vascular walls and interstitial regions, but barely detectable in the airway and vascular lumens (Figure S5A). Intense complement fixation was also observed in airway epithelial cells and vascular walls (Figure S5B). In

contrast, immune complexes and complement fixation were not evident in a normal lung biopsy (Figures 5B and 6B). Taken together, these results strongly suggest that intense immune complex formation and complement fixation associated with pathogenic antibodies and complement activation might be critical drivers of ARDS in fatal COVID-19. This is consistent with recent studies showing evidence of fatal COVID-19 vasculopathy accompanying deposition of immune complexes and/or complement components inside vascular walls in multiple organs (Magro et al., 2020; Roncati et al., 2020).

#### DISCUSSION

Based on the results of our extensive kinetic analyses using respiratory specimens showing enhanced viral antigen-specific antibody responses and concomitant complement activation, we propose that sustained eosinophil-mediated inflammation is followed by Th2-biased adaptive immune responses in critical COVID-19. Overt antibody responses together with complement activation potentially contribute to the progression and pathogenesis of critical COVID-19. However, significant infiltration of eosinophils into lungs of COVID-19 patients during the acute phase of infection can be either protective or detrimental (Lindsley et al., 2020). Although peripheral blood eosinopenia at initial presentation might be associated with critical COVID-19 as we and others observed in COVID-19 patients (see complete blood count results in Figure S6A) (Qin et al., 2020), sustained and enhanced levels of eosinophil-mediated inflammation in respiratory tracts of COVID-19 are consistently observed in critical cases (Figure 2E). Interestingly, rapid eosinophilic infiltration into infected lungs within 10 days after symptom onset was often observed in mild patients. In contrast, eosinophil infiltration is delayed but prolonged, and eosinophil-mediated inflammation is significantly increased as indicated by enhanced ECP and EDN responses, in respiratory tracts of severe pneumonic cases. Eosinophil responses during the early stage of viral infection can orchestrate antiviral responses to respiratory viruses by producing reactive oxygen species and eosinophil-derived RNases (EDN/RNase2 and ECP/RNase3) (Lindsley et al., 2020). However, sustained eosinophil-mediated inflammation may represent an acute type I hypersensitivity reaction, which is often functionally linked to a Th2-polarizing respiratory environment (De Giacomo et al., 2018). Enhanced TGF- $\beta$  responses, mast cell activation, and more prompt and robust viral antigen-specific antibody responses strongly support the potential pathogenic role of eosinophil-mediated inflammation and Th2-biased mucosal immunity in critical COVID-19 (Figure 3G) (Lucas et al., 2020). Several studies have recently reported an association of systemic eosinophil-mediated inflammation with various COVID-19-associated syndromes (Craver et al., 2020; Leis-Dosil et al., 2020). It is also notable that the levels of ECP in respiratory specimens from critical elderly patients are significantly higher than those from younger patients, suggesting a potential role of aging-associated inflammation in critical COVID-19 (Figure S1G). Therefore, host factor(s) specifically driving overt pulmonary inflammation caused by innate cellular activation in critical patients need to be further assessed in future studies.

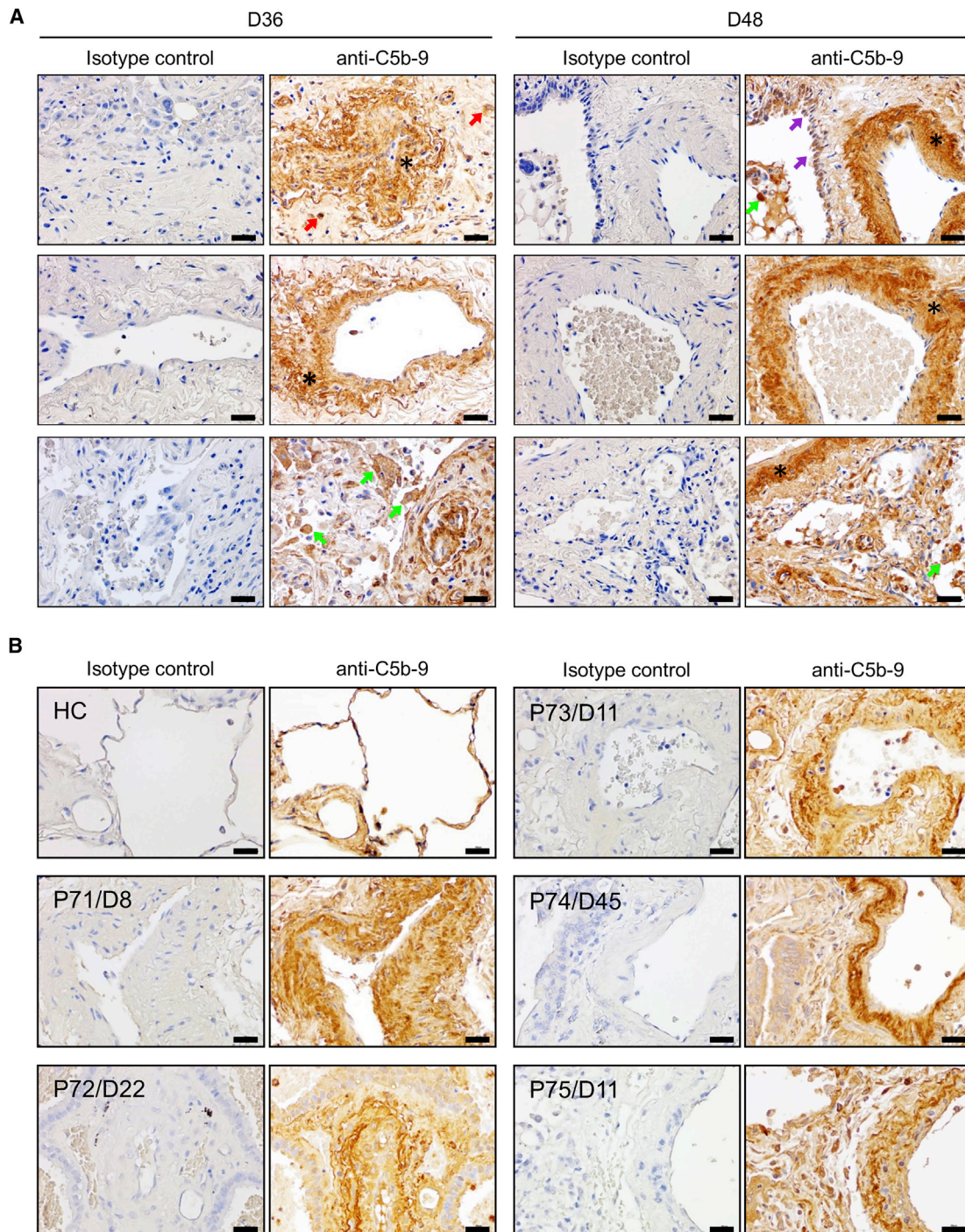
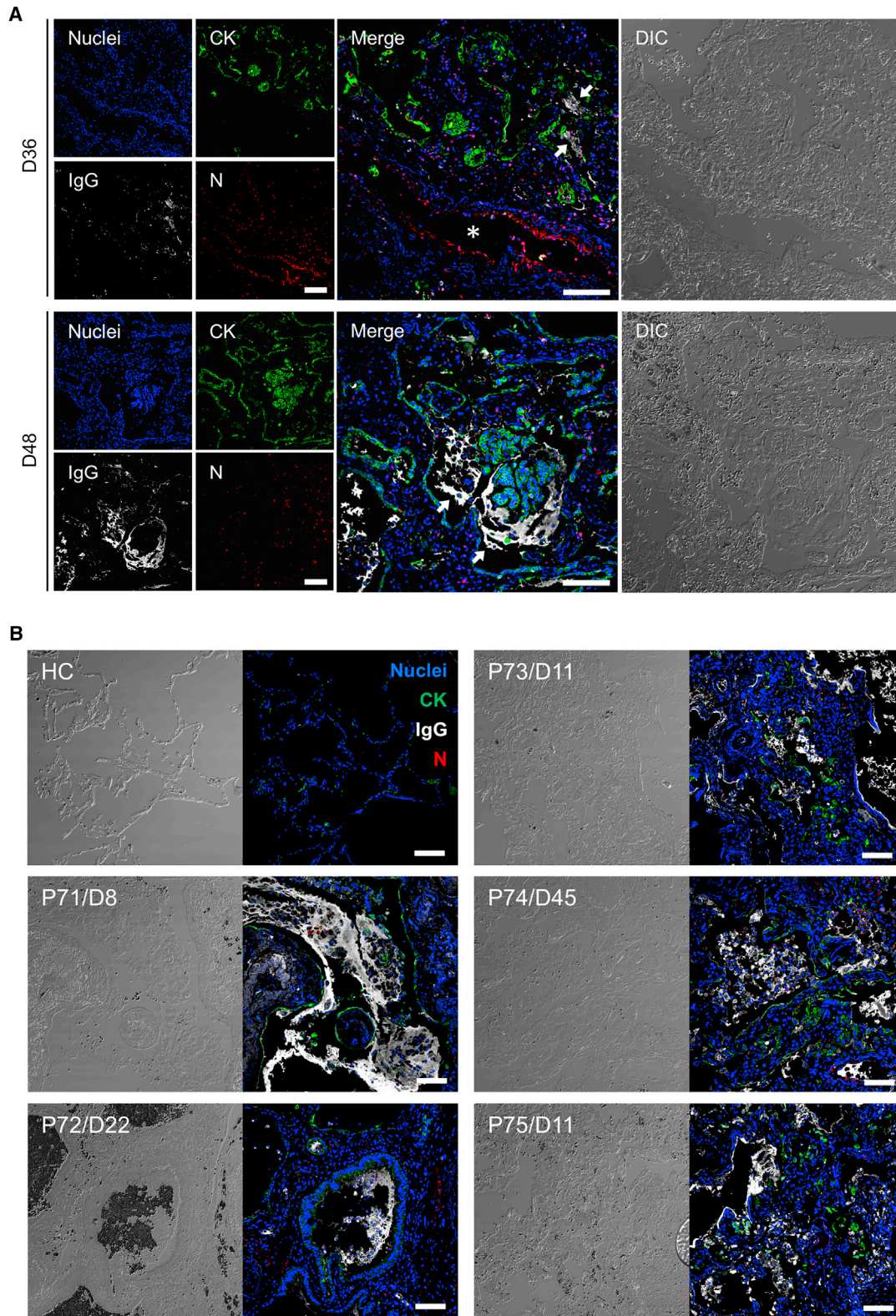


**Figure 5. Pathologic association of complement activation in lung biopsies from six fatal COVID-19 cases**

(A) Immunohistochemical detection of C5b-9 membrane attack complexes in pulmonary parenchyma of lung tissues from a fatal case, P15, obtained at the indicated times. Asterisks indicate the media layer of vascular walls; purple arrows indicate airway epithelial cells; green arrows indicate macrophages; and red arrows indicate lymphoplasmic cells. Scale bars, 100  $\mu$ m.

(B) Immunohistochemical detection of C5b-9 membrane attack complexes in pulmonary parenchyma of lung tissues from five fatal cases, P71–P75 (collection day after symptom onset indicated). HC, a normal lung biopsy. Scale bars, 100  $\mu$ m.



(legend on next page)

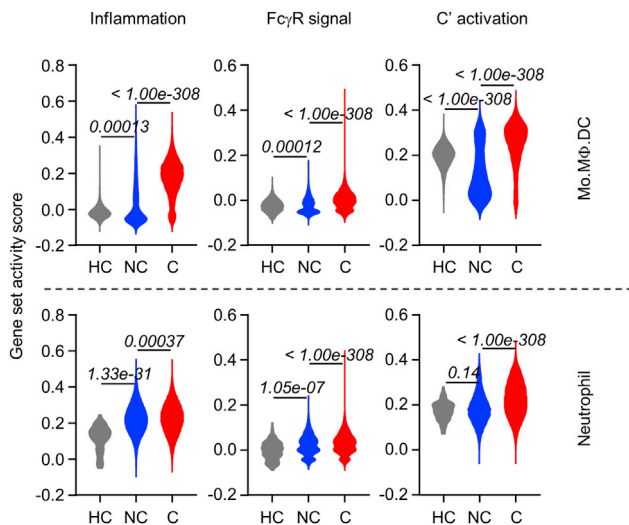


**Figure 7. Enhanced gene set signatures for Fc $\gamma$ R signaling and complement activation in myeloid cells of respiratory samples from critical COVID-19 cases**

Computed hallmark gene set activity scores of overall inflammation, Fc $\gamma$ R signaling, and complement activation for the indicated myeloid subsets.  $p$  values (two-tailed Mann-Whitney U test) for differences among HC and COVID-19 patients with NC or C symptoms are indicated.

Systemic corticosteroid therapy is generally considered to be the main treatment of acute eosinophilic pneumonia. Analysis of large open-label randomized trials with COVID-19 patients indicated that methylprednisolone significantly reduced mortality in ARDS patients (Philitt et al., 2002; Prescott and Rice, 2020). When we assessed the effect of corticosteroid therapy on ECP levels, a marker of eosinophil-mediated inflammation, in sputa samples ( $n = 21$ ) from our limited patient set, we noted a significant reduction in ECP levels, while neutrophil-mediated inflammation, as indicated by LCN levels ( $n = 18$ ), was not significantly changed (Figure S2G). The efficacy of steroid treatment on decreasing mortality risk and eosinophil-mediated inflammation suggests that critical COVID-19 pneumonia is, in fact, associated with acute eosinophil-mediated inflammation.

Recently, dysregulation of type I IFN responses has been proposed as one of the critical factors associated with COVID-19 severity (Acharya et al., 2020; Lee and Shin, 2020). Indeed, when we carefully analyzed gene set activity scores reported in two previous studies using respiratory leukocytes (Chua et al., 2020; Liao et al., 2020), a more robust type I IFN response was detected in critical COVID-19 (Figure S6A). Interestingly, type I IFN response in the pulmonary leukocytes in the critical group was initially suppressed during the first 10 days after symptom onset, but there was a more robust rebound thereafter when compared with non-critical cases (Figure S6A). We observed a

similar trend in gene set activity of Th2 responses (Figure S6D), whereas more enhanced M2 activity was consistently detected throughout the symptomatic period in the critical group (Figure S6C). Mechanistic and correlation studies using more datasets of pulmonary inflammation markers with defined clinical information are needed to elucidate decisive host innate factors for severe disease progression.

Our second critical finding is the potential role of enhanced antibody responses accompanying elevated complement activation in disease pathogenesis of severe COVID-19. Even though a recent study reported that defective Bcl-6<sup>+</sup> T follicular helper (Tfh) cell generation and dysregulated humoral immune induction early in COVID-19 limits the durability of antibody responses (Kaneke et al., 2020), another report showed that severe COVID-19 patients display hallmarks of extrafollicular B cell activation, which are strongly correlated with substantial expansion of antibody-secreting cells and early production of high concentration of SARS-CoV-2-specific antibodies (Woodruff et al., 2020). Indeed, more rapid and robust antibody responses specific to SARS-CoV-2 antigens, including spike and N, have been consistently observed in many other studies (Long et al., 2020; Wang et al., 2020b). Here, we confirmed enhanced antibody responses against viral N antigen in plasma and respiratory IgG responses in critical patients. In addition, kinetic analyses revealed earlier peak response (D10–D20) of systemic IgA and respiratory antibodies, followed by systemic IgG responses (peak at D20–D30) in critical cases. In contrast, all of these isotypes peaked at D20–D30 in plasma from non-critical group patients (Figure 4D). Moreover, complement activation was generally higher in the respiratory tract and systemic circulation of critical patients than in the non-critical group. This correlated well with the levels of IgM and IgG responses in the respiratory environment, suggesting increased activation of the antibody-dependent classical pathway. While the contribution of both alternative and lectin-dependent pathways during SARS-CoV-2 infection cannot be excluded (Magro et al., 2020), lower complement C1q levels in plasma from severe cases compared to those in mild cases (Wu et al., 2020) indicate that systemic C1q is depleted due to antibody-dependent classical complement pathway activation in severe cases. Nevertheless, it is unknown whether enhanced antibody responses and accompanying complement activation are directly and functionally associated with pathogenic progression of severe COVID-19 (Bournazos et al., 2020; Zohar and Alter, 2020). Enhanced antibody responses are not necessarily critical for antiviral immunity, since viral copy numbers in respiratory secretions declined to baseline during peak antibody responses (D20–D30), and there was no significant difference in viral loads between critical and non-critical patients during this period (Figure 1). In addition, systemic viremia has been rarely detected in most COVID-19 patients regardless of disease severity (Huang et al., 2020). Therefore, we suspected that Fc $\gamma$  receptor

**Figure 6. Pathologic association of immune complex deposition in lung biopsies from six fatal COVID-19 cases**

(A) Depositions of IgG immune complexes (white) in airways and blood vessels identified by immunofluorescence analysis of lung tissue from a fatal case, P15, at the indicated times after symptom onset. CK, pan-cytokeratin (green); N, SARS-CoV-2 N antigens (red); DIC, differential interference contrast. White arrows indicate depositions of IgG immune complexes in the luminal spaces; white asterisks indicate blood vessels. Nuclei are shown in blue. Scale bar, 100  $\mu$ m. (B) Depositions of IgG immune complexes in airways and blood vessels identified by immunofluorescence analysis of lung tissues obtained from five fatal cases, P71–P75 (collection day after symptom onset indicated). Scale bars, 100  $\mu$ m.

(Fc $\gamma$ R)-mediated inflammation upon crosslinking by immune complexes induces lung tissue damage through activation of the complement pathway and MAC formation (Bournazos et al., 2020). Since viral release from infected host cells rapidly decreases, rising antibodies might bind to cells expressing viral antigens. Infected host cells in the lungs of COVID-19 patients could be the primary targets for antigen-antibody immune complexes during the acute phase of COVID-19. Alternatively, a previous study suggests that defective B cell tolerance induced by sustained extrafollicular B cell responses may contribute to the production of autoreactive antibodies, which play a role in severe COVID-19 pathogenesis (Woodruff et al., 2020). Recently, Wang et al. (2020a) reported that COVID-19 patients exhibit a higher prevalence of autoantibodies against immunomodulatory proteins compared to uninfected controls. Regardless of target antigens, gradually increased IgG deposition on the luminal surfaces of airways and vasculatures observed in lung biopsies from fatal cases (Figure 6; Figure S4B) strongly supports the pathogenic role of the immune complex-mediated pathway. More robust antibody responses associated with immune complex-mediated inflammation, including complement activation, as well as effector leukocyte activation by engaging various members of Fc $\gamma$ R (Bournazos et al., 2020), may aggravate pulmonary inflammation in critical COVID-19 patients. When we analyzed scRNA-seq datasets from mononuclear phagocytes and neutrophils, there were significantly higher levels of hallmark gene set scores for both Fc $\gamma$ R signaling and complement activation in the critical group than in non-critical cases (Figure 7). These results clearly indicate a significant role of Fc $\gamma$ R signaling and complement activation in inflammatory responses and pathogenesis by phagocytic cells (Bournazos et al., 2020; Cugno et al., 2020; Merad and Martin, 2020).

In conclusion, our current kinetic analyses of respiratory specimens from COVID-19 patients clearly reveal an association of eosinophil-mediated pulmonary inflammation with severe pneumonic pathogenesis. These observations require further confirmation with extensive analysis of the pathogenesis of eosinophil-mediated inflammation and its association with the pathogenic role of antibody responses and complement activation in order to establish proper therapeutic strategies against respiratory distress often resulting in mortality in COVID-19.

## STAR★METHODS

Detailed methods are provided in the online version of this paper and include the following:

- KEY RESOURCES TABLE
- RESOURCE AVAILABILITY
  - Lead contact
  - Materials availability
  - Data and code availability
- EXPERIMENTAL MODEL AND SUBJECT DETAILS
  - Study participants
  - Ethics statement
- METHOD DETAILS
  - Processing and validation of respiratory specimens, and cytological analysis

- Quantitation of cytokines and chemokines
- Enzyme-linked immunosorbent assay (ELISA)
- Quantitation of viral loads
- Quantitation of complements
- Immunohistochemistry and immunofluorescence assay using lung biopsies
- Analysis of single-cell RNA-seq datasets of BALFs from COVID-19 patients
- QUANTIFICATION AND STATISTICAL ANALYSIS

## SUPPLEMENTAL INFORMATION

Supplemental information can be found online at <https://doi.org/10.1016/j.celrep.2021.109798>.

## ACKNOWLEDGMENTS

This work was supported by a grant from the National Research Foundation of Korea (grant no. 2021M3A9H5020761 and 2017M3A9E4061998) and a grant (2020ER53380) from Korea Center for Disease Control and Prevention, funded by the Government of South Korea. Y.-S.K., U.P., N.-Y.H., H.P., K.J., and J.-G.K. received a scholarship from the BK21-plus education program provided by the National Research Foundation of Korea.

## AUTHOR CONTRIBUTIONS

D.-M.K., Y.-S.K., and N.-H.C. conceived the study and analyzed the data. J.-W.S., Y.K., J.L., U.P., and N.-Y.H. performed most experiments and analyzed the data. J.K., S.-C.L., and Y.K.J. performed histopathological analysis. H.P., J.-W.L., H.-J.R., and J.-G.K. helped with immunoassays. N.R.Y., D.Y.K., S.H.Y., Y.S.N., D.S.M., C.-M.K., H.J., J.K., S.C., K.M.S., J.Y.M., J.-Y.C., and S.K. collected clinical specimens and analyzed clinical records. K.J., H.-J.K., and W.-Y.P. analyzed the RNA-seq data. S.R.H. and M.-S.L. performed analysis of complement activation. H.-W.S., H.-Y.K., and C.-H.C. provided research materials and revised the paper. D.-M.K., Y.-S.K., and N.-H.C. wrote the paper and supervised experimental processes.

## DECLARATION OF INTERESTS

The authors declare no competing interests.

Received: November 4, 2020

Revised: January 25, 2021

Accepted: September 14, 2021

Published: October 5, 2021

## REFERENCES

- Acharya, D., Liu, G., and Gack, M.U. (2020). Dysregulation of type I interferon responses in COVID-19. *Nat. Rev. Immunol.* 20, 397–398.
- Borsutzky, S., Cazac, B.B., Roes, J., and Guzmán, C.A. (2004). TGF- $\beta$  receptor signaling is critical for mucosal IgA responses. *J. Immunol.* 173, 3305–3309.
- Bournazos, S., Gupta, A., and Ravetch, J.V. (2020). The role of IgG Fc receptors in antibody-dependent enhancement. *Nat. Rev. Immunol.* 20, 633–643.
- Carvelli, J., Demaria, O., Vély, F., Batista, L., Chouaki Benmansour, N., Fares, J., Carpentier, S., Thibault, M.L., Morel, A., Remark, R., et al.; Explore COVID-19 IPH group; Explore COVID-19 Marseille Immunopole group (2020). Association of COVID-19 inflammation with activation of the C5a-C5aR1 axis. *Nature* 588, 146–150.
- Chua, R.L., Lukassen, S., Trump, S., Hennig, B.P., Wendisch, D., Pott, F., Debnath, O., Thürmann, L., Kurth, F., Völker, M.T., et al. (2020). COVID-19 severity correlates with airway epithelium-immune cell interactions identified by single-cell analysis. *Nat. Biotechnol.* 38, 970–979.

- Craver, R., Huber, S., Sandomirsky, M., McKenna, D., Schieffelin, J., and Finger, L. (2020). Fatal eosinophilic myocarditis in a healthy 17-year-old male with severe acute respiratory syndrome coronavirus 2 (SARS-CoV-2). *Fetal Pediatr. Pathol.* **39**, 263–268.
- Cugno, M., Meroni, P.L., Gualtierotti, R., Griffini, S., Grovetti, E., Torri, A., Panigada, M., Aliberti, S., Blasi, F., Tedesco, F., and Peyvandi, F. (2020). Complement activation in patients with COVID-19: A novel therapeutic target. *J. Allergy Clin. Immunol.* **146**, 215–217.
- De Giacomo, F., Vassallo, R., Yi, E.S., and Ryu, J.H. (2018). Acute eosinophilic pneumonia. Causes, diagnosis, and management. *Am. J. Respir. Crit. Care Med.* **197**, 728–736.
- Gubernatorova, E.O., Gorshkova, E.A., Polinova, A.I., and Drutskaia, M.S. (2020). IL-6: Relevance for immunopathology of SARS-CoV-2. *Cytokine Growth Factor Rev.* **53**, 13–24.
- Huang, C., Wang, Y., Li, X., Ren, L., Zhao, J., Hu, Y., Zhang, L., Fan, G., Xu, J., Gu, X., et al. (2020). Clinical features of patients infected with 2019 novel coronavirus in Wuhan, China. *Lancet* **395**, 497–506.
- Kahloon, R.A., Xue, J., Bhargava, A., Csizmadia, E., Otterbein, L., Kass, D.J., Bon, J., Soejima, M., Levesque, M.C., Lindell, K.O., et al. (2013). Patients with idiopathic pulmonary fibrosis with antibodies to heat shock protein 70 have poor prognoses. *Am. J. Respir. Crit. Care Med.* **187**, 768–775.
- Kaneko, N., Kuo, H.H., Boucau, J., Farmer, J.R., Allard-Chamard, H., Mahajan, V.S., Piechocka-Trocha, A., Lefteri, K., Osborn, M., Bals, J., et al.; Massachusetts Consortium on Pathogen Readiness Specimen Working Group (2020). Loss of Bcl-6-expressing T follicular helper cells and germinal centers in COVID-19. *Cell* **183**, 143–157.e13.
- Lee, J.S., and Shin, E.C. (2020). The type I interferon response in COVID-19: Implications for treatment. *Nat. Rev. Immunol.* **20**, 585–586.
- Leis-Dosil, V.M., Saenz Vicente, A., and Lorigo-Cortes, M.M. (2020). Eosinophilic panniculitis associated with COVID-19. *Actas Dermosifiliogr (Eng. Ed.)* **111**, 804–805.
- Li, H., Xiang, X., Ren, H., Xu, L., Zhao, L., Chen, X., Long, H., Wang, Q., and Wu, Q. (2020). SAA is a biomarker to distinguish the severity and prognosis of coronavirus disease 2019 (COVID-19). *J. Infect.* **80**, P646–P655.
- Liao, M., Liu, Y., Yuan, J., Wen, Y., Xu, G., Zhao, J., Cheng, L., Li, J., Wang, X., Wang, F., et al. (2020). Single-cell landscape of bronchoalveolar immune cells in patients with COVID-19. *Nat. Med.* **26**, 842–844.
- Lindsley, A.W., Schwartz, J.T., and Rothenberg, M.E. (2020). Eosinophil responses during COVID-19 infections and coronavirus vaccination. *J. Allergy Clin. Immunol.* **146**, 1–7.
- Long, Q.X., Liu, B.Z., Deng, H.J., Wu, G.C., Deng, K., Chen, Y.K., Liao, P., Qiu, J.F., Lin, Y., Cai, X.F., et al. (2020). Antibody responses to SARS-CoV-2 in patients with COVID-19. *Nat. Med.* **26**, 845–848.
- Lucas, C., Wong, P., Klein, J., Castro, T.B.R., Silva, J., Sundaram, M., Ellingson, M.K., Mao, T., Oh, J.E., Israelow, B., et al.; Yale IMPACT Team (2020). Longitudinal analyses reveal immunological misfiring in severe COVID-19. *Nature* **584**, 463–469.
- Magro, C., Mulvey, J.J., Berlin, D., Nuovo, G., Salvatore, S., Harp, J., Baxter-Stoltzfus, A., and Laurence, J. (2020). Complement associated microvascular injury and thrombosis in the pathogenesis of severe COVID-19 infection: A report of five cases. *Transl. Res.* **220**, 1–13.
- Mazzoni, A., Salvati, L., Maggi, L., Capone, M., Vanni, A., Spinicci, M., Mencarini, J., Caporale, R., Peruzzi, B., Antonelli, A., et al. (2020). Impaired immune cell cytotoxicity in severe COVID-19 is IL-6 dependent. *J. Clin. Invest.* **130**, 4694–4703.
- Merad, M., and Martin, J.C. (2020). Pathological inflammation in patients with COVID-19: a key role for monocytes and macrophages. *Nat. Rev. Immunol.* **20**, 355–362.
- Pechous, R.D. (2017). With friends like these: The complex role of neutrophils in the progression of severe pneumonia. *Front. Cell. Infect. Microbiol.* **7**, 160.
- Persson, C. (2019). Airways exudation of plasma macromolecules: Innate defense, epithelial regeneration, and asthma. *J. Allergy Clin. Immunol.* **143**, 1271–1286.
- Philit, F., Etienne-Mastroianni, B., Parrot, A., Guérin, C., Robert, D., and Cordier, J.F. (2002). Idiopathic acute eosinophilic pneumonia: A study of 22 patients. *Am. J. Respir. Crit. Care Med.* **166**, 1235–1239.
- Pont, F., Tosolini, M., and Fournié, J.J. (2019). Single-Cell Signature Explorer for comprehensive visualization of single cell signatures across scRNA-seq datasets. *Nucleic Acids Res.* **47**, e133.
- Prescott, H.C., and Rice, T.W. (2020). Corticosteroids in COVID-19 ARDS: Evidence and hope during the pandemic. *JAMA* **324**, 1292–1295.
- Qin, C., Zhou, L., Hu, Z., Zhang, S., Yang, S., Tao, Y., Xie, C., Ma, K., Shang, K., Wang, W., et al. (2020). Dysregulation of immune response in patients with COVID-19 in Wuhan, China. *Clin. Infect. Dis.* **71**, 762–768.
- Ricklin, D., Reis, E.S., and Lambris, J.D. (2016). Complement in disease: A defense system turning offensive. *Nat. Rev. Nephrol.* **12**, 383–401.
- Roncati, L., Ligabue, G., Fabbiani, L., Malagoli, C., Gallo, G., Lusenti, B., Nasillo, V., Manenti, A., and Maiorana, A. (2020). Type 3 hypersensitivity in COVID-19 vasculitis. *Clin. Immunol.* **217**, 108487.
- Rosenberg, H.F., Dyer, K.D., and Foster, P.S. (2013). Eosinophils: Changing perspectives in health and disease. *Nat. Rev. Immunol.* **13**, 9–22.
- Shoenfeld, Y. (2020). Corona (COVID-19) time musings: Our involvement in COVID-19 pathogenesis, diagnosis, treatment and vaccine planning. *Autoimmun. Rev.* **19**, 102538.
- Wang, E.Y., Mao, T., Klein, J., Dai, Y., Huck, J.D., Liu, F., Zheng, N.S., Zhou, T., Israelow, B., Wong, P., et al. (2020a). Diverse functional autoantibodies in patients with COVID-19. *medRxiv*.
- Wang, Y., Zhang, L., Sang, L., Ye, F., Ruan, S., Zhong, B., Song, T., Alshukairi, A.N., Chen, R., Zhang, Z., et al. (2020b). Kinetics of viral load and antibody response in relation to COVID-19 severity. *J. Clin. Invest.* **130**, 5235–5244.
- Woodruff, M.C., Ramonell, R.P., Nguyen, D.C., Cashman, K.S., Saini, A.S., Haddad, N.S., Ley, A.M., Kyu, S., Howell, J.C., Ozturk, T., et al. (2020). Extra-follicular B cell responses correlate with neutralizing antibodies and morbidity in COVID-19. *Nat. Immunol.* **21**, 1506–1516.
- Wu, Y., Huang, X., Sun, J., Xie, T., Lei, Y., Muhammad, J., Li, X., Zeng, X., Zhou, F., Qin, H., et al. (2020). Clinical characteristics and immune injury mechanisms in 71 patients with COVID-19. *MSphere* **5**, e00362-20.
- Yang, X., Yu, Y., Xu, J., Shu, H., Xia, J., Liu, H., Wu, Y., Zhang, L., Yu, Z., Fang, M., et al. (2020). Clinical course and outcomes of critically ill patients with SARS-CoV-2 pneumonia in Wuhan, China: A single-centered, retrospective, observational study. *Lancet Respir. Med.* **8**, 475–481.
- Zeng, Z., Xu, L., Xie, X.Y., Yan, H.L., Xie, B.J., Xu, W.Z., Liu, X.A., Kang, G.J., Jiang, W.L., and Yuan, J.P. (2020). Pulmonary pathology of early phase COVID-19 pneumonia in a patient with a benign lung lesion. *Histopathology* **77**, 823–831.
- Zhou, F., Yu, T., Du, R., Fan, G., Liu, Y., Liu, Z., Xiang, J., Wang, Y., Song, B., Gu, X., et al. (2020). Clinical course and risk factors for mortality of adult inpatients with COVID-19 in Wuhan, China: A retrospective cohort study. *Lancet* **395**, 1054–1062.
- Zohar, T., and Alter, G. (2020). Dissecting antibody-mediated protection against SARS-CoV-2. *Nat. Rev. Immunol.* **20**, 392–394.

STAR★METHODS

KEY RESOURCES TABLE

REAGENT or RESOURCE	SOURCE	IDENTIFIER
<b>Antibodies</b>		
Mouse anti-Human CD31 (clone JC70A)	Agilent	Cat#M0823, RRID: AB_2114471
Mouse anti-Human Cytokeratin (clone AE1/AE3)	Agilent	Cat#M3515, RRID: AB_2132885
Anti-C5b-9 antibody (rabbit polyclonal)	Abcam	Cat#ab55811, RRID:AB_879748
Anti-C3b antibody (mouse monoclonal)	Thermo Fisher Scientific	Cat#MA1-70054, RRID:AB_1073822
Rabbit (DA1E) mAb IgG XP® Isotype Control	Cell Signaling Technology	Cat#3900, RRID:AB_1550038
Mouse (G3A1) mAb IgG1 Isotype control	Cell Signaling Technology	Cat#5415, RRID:AB_10829607
Goat anti-Human IgG (H+L), HRP conjugate	Promega	Cat#W4031, RRID:AB_430835
Mouse anti-Human IgG1 Fc, HRP conjugate	Southern Biotech	Cat#9054-05, RRID:AB_2796627
Mouse anti-Human IgG2 Fc, HRP conjugate	Southern Biotech	Cat# 9070-05, RRID:AB_2796633
Mouse anti-human IgG3 Hinge, HRP conjugate	Southern Biotech	Cat#9210-05, RRID:AB_2796699
Mouse anti-Human IgG4, HRP conjugate	Southern Biotech	Cat#9200-05, RRID:AB_2796691
Goat anti-Human IgA, HRP conjugate	Southern Biotech	Cat#2050-05, RRID:AB_2687526
Goat anti-Human IgM, HRP conjugate	Southern Biotech	Cat#2020-05, RRID:AB_2687526
Goat anti-Human IgG (H+L), Alexa fluor 488	Thermo Fisher Scientific	Cat#A11013, RRID:AB_2534080
Goat anti-Mouse IgG (H+L), Alexa fluor 633	Thermo Fisher Scientific	Cat#A21052, RRID:AB_2535719
Donkey anti-rabbit IgG (H+L), Alexa fluor 594	Thermo Fisher Scientific	Cat#A21207, RRID:AB_141637
Rabbit serum against SARS-CoV-2 N protein	Abclone	N/A
<b>Biological samples</b>		
Nasopharyngeal swabs, sputa, bronchoalveolar lavage fluids, plasma, and lung tissues from COVID-19 patients	Chosun University Hospital and Chungnam National University Hospital	N/A
Lung tissue sections from healthy volunteers	Seoul National University Hospital	N/A
Plasma from healthy donors	Chungnam National University Hospital	N/A
<b>Chemicals, peptides, and recombinant proteins</b>		
Protease Inhibitor Cocktail Set III	Millipore	Cat#535140
Dithiothreitol (DTT)	Sigma-Aldrich	Cat#9779
3,3',5,5'-tetramethylbenzidine (TMB)	KPL	Cat#5120-0053
Phosphoric acid	Sigma-Aldrich	Cat#466123
Hematoxylin solution	Merck	Cat#105174
Eosin Y Alcoholic	Mirax	Cat#3610
Xylenes	Sigma-Aldrich	Cat#534056
Tri-sodium citrate	Sigma-Aldrich	Cat#C8532
Sudan Black B	Sigma-Aldrich	Cat#199664
4,6-diamidino-2-phenylindole	Thermo Fisher Scientific	Cat#D3571
Human BD Fc Block	BD Biosciences	Cat#564220
Albumin, Bovine serum, fraction V	Mpbio	Cat#9048-46-8
Skim Milk	BD Difco	Cat#232100
Recombinant SARS-CoV-2 N protein	BIONICS	N/A
BLOXALL Endogenous Peroxidase and Alkaline Phosphatase Blocking Solution	VECTOR LABORATORIES	Cat#SP-6000
ImmPACT DAB Peroxidase (HRP) Substrate	VECTOR LABORATORIES	Cat#SK-4105

(Continued on next page)

**Continued**

REAGENT or RESOURCE	SOURCE	IDENTIFIER
<b>Critical commercial assays</b>		
PowerPrep TM Viral DNA/RNA Extraction Kit	Kogenebiotech	Cat#IE0007
PowerChekTM 2019-nCoV Real-time PCR Kit	Kogenebiotech	Cat#R6900T
Human multiplex-1 (hMagLxSA (23 PLEX))	R&D Systems	Cat#LXSAHM-23
Human multiplex-2 (CCL5)	R&D Systems	Cat#LXSAHM-01
Human multiplex-3 (CXCL16)	R&D Systems	Cat#LXSAHM-01
Human multiplex-4 (TGFB1)	R&D Systems	Cat#LTGM00(100)
Human alpha 2 Macroglobulin ELISA Kit	Abcam	Cat#108888
Human IL-33 ELISA Kit	Thermo Fisher Scientific	Cat#BMS2048
Human Lipocalin-2 ELISA Kit	Abcam	Cat#113326
Human ribonuclease, RNase A family, 2 (liver, eosinophil-derived neurotoxin) (RNASE2) ELISA kit	Cusabio	Cat#CSB-E17923h
Human mast cell tryptase, MCT ELISA Kit	Cusabio	Cat#CSB-E09012h
IMMULITE2000 ECP	Siemens	Cat#L2KE02
CALPROLAB Calprotectin ELISA (ALP)	Calpor AS	Cat#CALP0170
Complement C3a Human ELISA Kit	Thermo Fisher Scientific	Cat#BMS2089
ImmPRESS Excel Amplified HRP Polymer Staining Kit (Anti-Rabbit IgG)	VECTOR LABORATORIES	Cat#MP-7601
ImmPRESS Excel Amplified HRP Polymer Staining Kit (Anti-Mouse IgG)	VECTOR LABORATORIES	Cat#MP-7602
<b>Deposited data</b>		
BALF single cell RNA seq (scRNA-seq) datasets	<a href="#">Liao et al., 2020</a>	GEO: GSE145926
COVID19 airway epithelium-immune cell single-cell RNA seq	<a href="#">Chua et al., 2020</a>	<a href="https://figshare.com/articles/dataset/COVID-19_severity_correlates_with_airway_epithelium-immune_cell_interactions_identified_by_single-cell_analysis/12436517">https://figshare.com/articles/dataset/COVID-19_severity_correlates_with_airway_epithelium-immune_cell_interactions_identified_by_single-cell_analysis/12436517</a>
Inflammation hallmark gene set		<a href="https://www.gsea-msigdb.org/gsea/msigdb/cards/HALLMARK_INFLAMMATORY_RESPONSE">https://www.gsea-msigdb.org/gsea/msigdb/cards/HALLMARK_INFLAMMATORY_RESPONSE</a>
Complement activation hallmark gene set		<a href="https://www.gsea-msigdb.org/gsea/msigdb/cards/HALLMARK_COMPLEMENT">https://www.gsea-msigdb.org/gsea/msigdb/cards/HALLMARK_COMPLEMENT</a>
Reactome Fc $\gamma$ R activation (R-HSA-2029481)		<a href="https://reactome.org/PathwayBrowser/#/R-HSA-2029480&amp;SEL=R-HSA-2029481&amp;PATH=R-HSA-168256,R-HSA-168249&amp;DTAB=MT">https://reactome.org/PathwayBrowser/#/R-HSA-2029480&amp;SEL=R-HSA-2029481&amp;PATH=R-HSA-168256,R-HSA-168249&amp;DTAB=MT</a>
Classical M1 versus alternative M2 macrophage down (GSE5099_3808_200_DN)		<a href="https://www.gsea-msigdb.org/gsea/msigdb/cards/GSE5099_CLASSICAL_M1_VS_ALTERNATIVE_M2_MACROPHAGE_DN">https://www.gsea-msigdb.org/gsea/msigdb/cards/GSE5099_CLASSICAL_M1_VS_ALTERNATIVE_M2_MACROPHAGE_DN</a>
Classical M1 versus alternative M2 macrophage up (GSE5099_3808_200_UP)		<a href="https://www.gsea-msigdb.org/gsea/msigdb/cards/GSE5099_CLASSICAL_M1_VS_ALTERNATIVE_M2_MACROPHAGE_UP">https://www.gsea-msigdb.org/gsea/msigdb/cards/GSE5099_CLASSICAL_M1_VS_ALTERNATIVE_M2_MACROPHAGE_UP</a>
Response to Type I IFN (GO:0034340)		<a href="https://www.gsea-msigdb.org/gsea/msigdb/cards/GOBP_RESPONSE_TO_TYPE_I_INTERFERON">https://www.gsea-msigdb.org/gsea/msigdb/cards/GOBP_RESPONSE_TO_TYPE_I_INTERFERON</a>
Positive regulation of T-helper type 1 immune response (GO:0002827)		<a href="http://www.informatics.jax.org/vocab/gene_ontology/GO:0002827">http://www.informatics.jax.org/vocab/gene_ontology/GO:0002827</a>
Positive regulation of T-helper type 2 immune response (GO:0002830)		<a href="http://www.informatics.jax.org/vocab/gene_ontology/GO:0002830">http://www.informatics.jax.org/vocab/gene_ontology/GO:0002830</a>
Positive regulation of T-helper 17 type immune response (GO: 2000318)		<a href="http://www.informatics.jax.org/vocab/gene_ontology/GO:2000318">http://www.informatics.jax.org/vocab/gene_ontology/GO:2000318</a>
<b>Software and algorithms</b>		
R (version 4.0.5)	<a href="https://cran.r-project.org/">https://cran.r-project.org/</a>	<a href="https://cran.r-project.org/">https://cran.r-project.org/</a>
corrplot 0.84 R package		<a href="https://github.com/taiyun/corrplot">https://github.com/taiyun/corrplot</a>
Seurat (version 3.1.4) package		<a href="https://github.com/satijalab/seurat">https://github.com/satijalab/seurat</a>

(Continued on next page)

**Continued**

REAGENT or RESOURCE	SOURCE	IDENTIFIER
xPONENT software (version 4.3)	Luminex	<a href="https://www.luminexcorp.com/download/xponent-software-version/">https://www.luminexcorp.com/download/xponent-software-version/</a>
Fluoview31S-SW (version 2.5)	Olympus	<a href="https://www.olympus-lifescience.com/">https://www.olympus-lifescience.com/</a>
Magellan	TECAN	<a href="https://lifesciences.tecan.com/software-magellan">https://lifesciences.tecan.com/software-magellan</a>
Graph Pad Prism (version 5.01)	GraphPad	<a href="https://www.graphpad.com/">https://www.graphpad.com/</a>
Excel 2016	Microsoft	<a href="https://www.microsoft.com/">https://www.microsoft.com/</a>
CFX Manager Dx Software, version 3.1	Biorad	<a href="https://www.bio-rad.com/en-us/sku/1845000-cfx-manager-software?ID=1845000">https://www.bio-rad.com/en-us/sku/1845000-cfx-manager-software?ID=1845000</a>

**RESOURCE AVAILABILITY**

**Lead contact**

Further information and requests for resources and reagents should be directed to and will be fulfilled by the lead contact, Nam-hyuk Cho ([chonh@snu.ac.kr](mailto:chonh@snu.ac.kr)).

**Materials availability**

This study did not generate new unique reagents.

**Data and code availability**

- The published article includes all datasets generated or analyzed during this study.
- This paper does not report original code
- Any additional information required to reanalyze the data reported in this paper is available from the lead contact upon request.

**EXPERIMENTAL MODEL AND SUBJECT DETAILS**

**Study participants**

General information on the clinical courses and baseline characteristics of the COVID-19 patients included in this study are summarized in [Table S1](#) and [Figure S1](#). The patients were divided into two groups based on WHO severity definitions (<https://www.who.int/covid-19/information>). The non-critical group includes 50 patients who were asymptomatic, with mild respiratory symptoms but no detectable pneumonia, or with mild to severe pneumonia determined by chest imaging and clinical data. The critical group includes 25 patients who suffered from acute respiratory distress syndrome (ARDS), or other clinical conditions requiring high flow oxygen supply and/or mechanical ventilation. Among the critical group patients, all the patients survived and were discharged, except nine patients (P15, P68 - 75) who succumbed to death due to fatal ARDS. Lung biopsies were obtained from P15 at the indicated time and five fatal cases (P71 ~75) after death. The patients were also divided into two sets. Group 1 includes 15 patients (10 non-critical and 5 critical group patients) who provided blood and respiratory specimens at different time points after symptoms onset. Group 2 includes 60 patients (40 non-critical and 20 critical patients) and provided respiratory specimens during the acute phase of COVID-19.

**Ethics statement**

The current research was approved by the institutional review boards of Chosun University Hospital (IRB no.: 2020-02-011), Chungnam National University Hospital (IRB no.: CNUH2017-12-004), and Seoul National University Hospital (IRB no.: C-1509-103-705). This study was performed in accordance with the ethical standards laid down in the 1964 declaration of Helsinki and all subsequent revisions. This study was conducted with informed consent from patients or their legal guardians.

**METHOD DETAILS**

**Processing and validation of respiratory specimens, and cytological analysis**

Fractions of BALFs and sputa samples from the patients were treated with 0.1% DTT solution and smeared on glass slides immediately after transport to a biosafety level 3 laboratory in Seoul National University on the same day of collection. The slides were then fixed with 95% ethanol in a Coplin jar. After fixing the slides, hematoxylin and eosin (H&E) staining was performed. The presence and relative proportions of various leukocyte subsets were estimated under light microscope independently by two experienced

pathologists and consensus was reached under multi-head microscope. We excluded lower respiratory specimens for further analysis if they included more than 10% of squamous epithelial cells in order to reduce salivary contamination. BALFs and sputa for quantitative analysis were diluted two to five folds with PBS containing protease inhibitor cocktail (Sigma-Aldrich, St. Louis, MO, USA), depending on their initial volume, then stored at  $-150^{\circ}\text{C}$  in cryogenic freezer (SANYO, Bensenville, IL, USA) until use. Viral inactivation in respiratory samples was performed by gamma-irradiation (30 kGy) in dry ice pack. For quantitative analysis of soluble proteins, including cytokines, inflammatory markers, and antibodies, lower respiratory samples were rapidly thawed at  $37^{\circ}\text{C}$  water bath and centrifuged ( $10,000 \times g$ ) at  $4^{\circ}\text{C}$  for 10 min. Supernatants were collected and further centrifuged at  $10,000 \times g$  for 10 min, with this final supernatant used for further analysis. We validated plasma exudation in the lower respiratory specimens by measuring the concentration of  $\alpha 2$ -macroglobulin and albumin as indexes of plasma leakage.  $\alpha 2$ -macroglobulin in respiratory samples were measured by ELISA (Abcam, Cambridge, UK) and albumin levels were assessed by a colorimetric assay (detection limit: 0.1 g/dl, SCL healthcare, Yongin-si, Gyeonggi-do, South Korea).

### Quantitation of cytokines and chemokines

Cytokine/chemokine levels in human respiratory samples (BALFs and sputa) were measured by a luminex multiplex assay system (Luminex, Austin, TX, USA). Luminex assay was run according to the manufacturer's instructions, using a customized human cytokine multiplex panel (R&D Systems, Inc. Minneapolis, MN, USA). The panel included: CCL2/JE/MCP-1, CCL3/MIP-1 $\alpha$ , CCL4/MIP-1 $\beta$ , CCL5/RNATES, CCL11/Eotaxin, complement component C5a, CX3CL1/Fractalkine, CXCL9/MIG, CXCL10/IP-10/CRG-2, CXCL16, IFN- $\gamma$ , IL-1 $\alpha$ /IL-1F1, IL-2, IL-4, IL-5, IL-6, IL-7, IL-8/CXCL8, IL-10, IL-12/IL-23p40, IL-13, IL-15, IL-21, Periosin/OSF-2, TNF- $\alpha$ , TGF- $\beta$ , sCD163, and granzyme A. Assay plates were measured using a Luminex 100/200TM analyzer (Luminex, Austin, TX, USA). Standard curve for each cytokine/chemokine was drawn using the supplied cytokine/chemokine standard and determined with the best fit algorithm using MasterPlex QT 2010 software (MiraiBio, Hitachi, CA, USA). IL-33 (Invitrogen, Carlsbad, CA, USA), lipocalin-2 (Abcam), EDN, and MCT (Cusabio, Houston, TX, USA) were quantified using human ELISA kits according to the manufacturer's instruction. Concentration of ECP and calprotectin in respiratory specimens were measured via clinical diagnosis service from Seoul Clinical Laboratory (Seoul, Republic of Korea). Hierarchical clustering of the soluble markers was applied to group the cytokines into modules of significantly correlated ones, based on their concentrations. To assess statistical difference of the cytokine group activity between non-critical and critical cases, min-max normalized datasets were used for two-tailed Mann-Whitney U test.

### Enzyme-linked immunosorbent assay (ELISA)

To assess for SARS-CoV-2 N protein-specific antibody responses, 96-well immunoassay plates (Nunc, Waltham, MA, USA) were coated with 100  $\mu\text{L}$  of purified antigen at a concentration of 1  $\mu\text{g}/\text{mL}$  at  $4^{\circ}\text{C}$  overnight. The plates were then blocked for 2 h at room temperature (RT) with PBS containing 5% skim milk. One hundred microliters of serially diluted plasma or respiratory samples were incubated for 2 h at RT. After washing with PBS containing 0.05% Tween20 (0.05% PBST), horseradish peroxidase (HRP)-conjugated mouse anti-human IgG1, IgG2, IgG3, IgG4, IgG, IgM, or IgA antibody (Southern Biotech, Birmingham, AL, USA) was added and incubated for 1 h at RT. Wells were washed with 0.05% PBST and incubated with a 3,3',5,5'-tetramethylbenzidine (TMB) peroxidase substrate solution (KPL, Gaithersburg, MD, USA) for 10min. The reactions were stopped by addition of a 1 M phosphoric acid solution. Absorbance was measured at 450 nm using a microplate reader (Beckman Coulter, Brea, CA, USA). The cut-off titer for the ELISA was defined as the lowest titer showing an optical density (OD) over the mean OD plus  $3 \times$  standard deviation (s.d.) from three control plasma samples (diluted 1:10) collected from healthy volunteers or three respiratory specimens from pneumonia patients who were never diagnosed with COVID-19 in every 96 well assay plate.

### Quantitation of viral loads

Real-time reverse transcription-polymerase chain reaction (RT-PCR) assay for detection of SARS-CoV-2 was performed according to the manufacturer's instructions (Kogenebiotech, Seoul, South Korea). Total RNAs were obtained from nasopharyngeal and throat swab samples (upper respiratory tract) and sputa (lower respiratory tract). Primer sets targeting E and RdRP genes of SARS-CoV-2 were used with a cut-off cycle threshold (Ct) value of higher than 38 cycles.

### Quantitation of complements

Human complement assays were conducted using quantitative C3a and C5a ELISA kits according to the manufacturer's instructions (Thermo Fisher Scientific, Waltham, MA, USA). In brief, patients' plasma were incubated in microwells adsorbed with anti-human C3a or C5a coating antibody for 2 h at RT, washed 6 times, and incubated with a biotin-conjugated anti-human C3a or C5a antibody for 1 h. The plates were then washed 6 times followed by incubation with streptavidin-HRP for 1 h. After washing the wells, TMB substrate solution was added and further incubated at RT. The reaction was terminated by adding 1 M phosphoric acid and absorbance was measured with a TECAN microplate reader (TECAN, Mannedorf, Switzerland) at 450 nm.

### Immunohistochemistry and immunofluorescence assay using lung biopsies

Histopathological analysis of lung biopsies was performed after fixation in 10% formalin and embedding in paraffin. Tissue sections (4  $\mu\text{m}$  thickness) were stained with hematoxylin and eosin (H&E) and two experienced pathologists specialized in lung pathology evaluated the H&E slides under a light microscope (Olympus BX-53; Olympus, Tokyo, Japan). For immunohistochemistry

and immunofluorescence analysis, paraffin-embedded tissue sections were placed at 55°C overnight. Tissue sections were rehydrated by submerging in xylene sequentially for 15 min, 5 min, and 5 min, followed by immersion in 100%, 100%, 95%, 90%, 80%, and 70% ethanol in serial order, for 3 min per step. For antigen retrieval, the slides were soaked and heated in HIER buffer (10 mM Tri-sodium citrate, 0.05% Tween-20, pH 6) in the microoven for 20 min. After blocking with a buffer containing 5% BSA and Fc blocker (BD Biosciences) for 1 h at room temperature, autofluorescence emitted by lung tissues was inhibited by incubation with 0.1% Sudan Black solution for 20 min, followed by incubation with indicated antibody for 15 minutes. The antibodies used to detect specific antigens for immunostaining processes were rabbit polyclonal anti-SARA-CoV-2 N antibody was obtained from Sino biological (Beijing, China) and anti-CD31 and pan-cytokeratin (CK) antibodies purchased from DAKO (Carpinteria, CA, USA). Antibody binding to the cells in sections was detected using horseradish peroxidase (HRP) reaction kits (DAKO) for immunohistochemistry or Alexa488-, Alexa594-, Alexa-633 conjugated secondary antibodies (Molecular Probes) for immunofluorescence. Nuclear DNA was counterstained with 4,6-diamidino-2-phenylindole (DAPI). Confocal microscopy was performed using an OlympusFV3000 laser-scanning microscope (Olympus). All images were analyzed and processed using the Olympus Fluoview or Adobe Photoshop software.

### Analysis of single-cell RNA-seq datasets of BALFs from COVID-19 patients

We collected BALF single cell RNA seq (scRNA-seq) datasets from the Gene Expression Omnibus (GEO) under accession code GSE145926 and from FigShare ([https://figshare.com/articles/dataset/COVID-19\\_severity\\_correlates\\_with\\_airway\\_epithelium-immune\\_cell\\_interactions\\_identified\\_by\\_single-cell\\_analysis/12436517](https://figshare.com/articles/dataset/COVID-19_severity_correlates_with_airway_epithelium-immune_cell_interactions_identified_by_single-cell_analysis/12436517)). We applied quality control criteria to each dataset (mitochondrial gene percentage < 0.15). After filtering, a total single cell of 182,140 were used for analysis. To remove batch effects across the two datasets, we used multi canonical correlation analysis 3 (CCA3) in Seurat3 R package. Variably expressed genes were selected using the FindVariableGenes function in default parameters of Seurat v3.1.5. Cell clustering and Uniform Manifold Approximation and Projection (UMAP) visualization were performed using the FindClusters and RunUMAP functions, respectively. The annotations of cell identity for each cluster were defined by the expression of known marker genes: epithelial cells, EFHC1 and MLF1; T/NK cells, IL32, KLRB1, and STMN1; B cell, CD19 and MS4A1; neutrophils, LYN, FCGR3B, and ITGAX; monocyte/macrophage/dendritic cells, CD14, CCL2, CD68, FABP5, CD74, CLEC4C, KIT, CPA3, HPGD, and LTC4S. To score the hallmark gene sets for inflammation, complement activation, reactome Fc $\gamma$ R activation, classical M1 versus alternative M2 macrophage activation, positive regulation of Th1/2/17 immune response, and type I IFN response datasets were downloaded from MsigDB (<https://www.gsea-msigdb.org/gsea/msigdb>) using the AddModuleScore function provided by the Seurat package and analyzed.

### QUANTIFICATION AND STATISTICAL ANALYSIS

Data was analyzed using the Graph Pad Prism 5.01 software (GraphPad Software, La Jolla, CA, USA) and Microsoft Excel (Microsoft Office Professional Plus 2016). Statistical analyses were performed using a two-tailed Mann-Whitney U test, or one-way analysis of variance (ANOVA) followed by Newman-Keuls t test for comparisons of values among different groups. Spearman's rank test or Pearson correlation test was used to analyze the correlation between variables. A *p-value* of < 0.05 was considered statistically significant.